ARTICLES
https://doi.org/10.1038/s41593-022-01065-x

nature neuroscience

Hypothalamic modulation of adult hippocampal neurogenesis in mice confers activity-dependent regulation of memory and anxiety-like behavior

Ya-Dong Li[1,2,6], Yan-Jia Luo[1,2,6], Ze-Ka Chen[1,2,3], Luis Quintanilla[1,2,4], Yoan Cherasse[5], Libo Zhang[1], Michael Lazarus[5], Zhi-Li Huang[3] and Juan Song[1,2] ✉

Adult hippocampal neurogenesis plays a critical role in memory and emotion processing, and this process is dynamically regulated by neural circuit activity. However, it remains unknown whether manipulation of neural circuit activity can achieve sufficient neurogenic effects to modulate behavior. Here we report that chronic patterned optogenetic stimulation of supramammillary nucleus (SuM) neurons in the mouse hypothalamus robustly promotes neurogenesis at multiple stages, leading to increased production of neural stem cells and behaviorally relevant adult-born neurons (ABNs) with enhanced maturity. Functionally, selective manipulation of the activity of these SuM-promoted ABNs modulates memory retrieval and anxiety-like behaviors. Furthermore, we show that SuM neurons are highly responsive to environmental novelty (EN) and are required for EN-induced enhancement of neurogenesis. Moreover, SuM is required for ABN activity-dependent behavioral modulation under a novel environment. Our study identifies a key hypothalamic circuit that couples novelty signals to the production and maturation of ABNs, and highlights the activity-dependent contribution of circuit-modified ABNs in behavioral regulation.

The hippocampus has considerable importance in regard to memory and emotion. One of the most striking features of this brain region is its unique capacity for adult neurogenesis, in which new neurons are generated throughout adulthood in the dentate gyrus (DG) where they mature and functionally integrate into existing circuitry[1–3]. These young adult-born neurons (ABNs) undergo a critical period of heightened synaptic plasticity 4–6 weeks after birth, during which they make distinct contributions to hippocampus-dependent learning and memory[4–9]. Therefore, strategies that positively modulate adult hippocampal neurogenesis (AHN) may benefit hippocampal functions.

Common strategies for enhancement of AHN include running[10], enriched environments[11] and pharmacological antidepressants[12]. However, these strategies impact multiple brain regions and cell types, so the mechanisms underlying enhanced AHN remain unclear. Other strategies involve manipulation of candidate genes in neural stem/progenitor cells or ABNs. Although studies have shown efficacy of these strategies in behavioral modulation in rodent models[13], the translational potential of these strategies is limited due to the technical challenges associated with cell-type-specific gene targeting in humans.

It is well established that AHN is dynamically regulated by neural circuit activity[14–16]. Compared with previous strategies for enhancement of AHN, neural circuits can convey input-specific information to multiple neurogenesis stages ranging from radial neural stem cells (rNSCs) to immature neurons for maximal modulation of behavior. Importantly, neural circuits can be targeted by deep brain stimulation, which has been widely used to treat symptoms associated with neurological and psychiatric disorders[17–19]. In the past few years we have made tremendous progress toward understanding activity-dependent regulation of the early stages of AHN by distinct neural circuits[20–24]. It remains unknown whether circuit-based enhancement of neurogenesis is sufficient to modify hippocampus-dependent behaviors.

Recent studies from our team and others have demonstrated that neurons in the SuM of the hypothalamus send dense axonal projections to the DG to regulate spatial memory performance[25,26]. SuM neurons also regulate hippocampal theta rhythm[27–29], sleep–wake cycles[30], behavioral responses to novelty signals[26] and locomotion[31]. To date, the role of SuM in regulation of AHN has never been investigated. In this study we utilized slice electrophysiology to examine the effects of SuM-DG inputs on neurogenesis stages ranging from rNSCs to immature neurons. We demonstrate that the SuM provides glutamatergic inputs onto rNSCs, followed by GABAergic inputs onto immature neurons, and finally, dual GABAergic/glutamatergic inputs onto behaviorally relevant ABNs. Importantly, chronic patterned optogenetic stimulation of SuM neurons robustly promoted neurogenesis at multiple stages, leading to increased production of rNSCs and behaviorally relevant ABNs with enhanced maturity. Functionally, we found that selective manipulation of the activity of SuM-modified ABNs further modulated memory retrieval and anxiety-like behavior when compared with control ABN activity-mediated behaviors. Furthermore, our in vivo fiber photometry and electrophysiological recordings showed that DG-projecting SuM neurons respond to environmental novelty with increased activity and firing frequency. Finally, we took a loss-of-function approach by ablating SuM neurons and showed that SuM is required for the production and maturation of ABNs at

[1]Department of Pharmacology, University of North Carolina at Chapel Hill, Chapel Hill, NC, USA. [2]Neuroscience Center, University of North Carolina at Chapel Hill, Chapel Hill, NC, USA. [3]Department of Pharmacology, School of Basic Medical Sciences; State Key Laboratory of Medical Neurobiology and MOE Frontiers Center for Brain Science, and Institutes of Brain Science, Fudan University, Shanghai, China. [4]Neuroscience Curriculum, University of North Carolina at Chapel Hill, Chapel Hill, NC, USA. [5]International Institute for Integrative Sleep Medicine (WPI-IIIS) and Faculty of Medicine, University of Tsukuba, Tsukuba, Japan. [6]These authors contributed equally: Ya-Dong Li, Yan-Jia Luo. ✉e-mail: juansong@email.unc.edu

baseline and under a novel environment. In addition, we showed that SuM is required for ABN activity-dependent behavioral modulation under the novel environment.

Results

Stimulation of SuM-DG projections depolarizes rNSCs through glutamate transmission. Recent studies from our team and others have shown dense SuM axonal projections in the supragranular layer of the DG that innervate mature granule cells (GCs)[29,32]. Whether SuM-DG projections form functional connections with rNSCs is unknown. To address this, we first examined the morphological association of SuM-DG projections and rNSCs by delivering AAV-CaMKII-mCherry to the lateral SuM of Nestin-GFP mice (Fig. 1a). SuM neurons are known to be reliably labeled by CaMKII-promoter-driven adeno-associated viruses (AAVs)[25,27]. Confocal images and three-dimensional (3D) reconstruction revealed close associations between rNSC bushy processes and SuM-DG projections (Fig. 1b–d). To address whether there are functional connections, we performed ChR2-assisted whole-cell recording in acute slices from Nestin-GFP mice[33] injected with AAV-CaMKII-ChR2-mCherry in the lateral SuM (Fig. 1e). Nestin-GFP$^+$ cells include type 1 rNSCs and type 2 progenitors with distinct morphological and electrophysiological properties (Fig. 1f,n and Extended Data Fig. 1a,b). We first recorded GFP$^+$ rNSCs upon patterned optogenetic stimulation of SuM-DG terminals under both current and voltage-clamp mode. Optogenetic stimulation of SuM-DG projections induced inward currents under voltage-clamp mode (Fig. 1g) and depolarization under current-clamp mode (Fig. 1h) in rNSCs. Of note, because rNSCs do not have synapses, light-evoked responses exhibit slow tonic characteristics.

SuM-DG terminals express both vesicular GABA transporter (Vgat) and vesicular glutamate transporter 2 (Vglut2)[34], and are capable of coreleasing glutamate and GABA[25,29]. Therefore, we sought to identify whether GABA and/or glutamate contribute to light-evoked responses in rNSCs. In the presence of the $GABA_AR$ antagonist bicuculline (BIC), amplitudes of light-evoked currents remained unchanged (Fig. 1i,j), suggesting that SuM GABA signaling is not involved. In contrast, a significant reduction in the amplitudes of light-evoked currents in rNSCs was observed in the presence of ionotropic glutamate receptor (iGluR) antagonists NBQX (AMPAR antagonist) and APV (NMDAR antagonist) (Fig. 1k–m). Because group 1 metabotropic glutamate receptors (mGluR) can also mediate rNSC depolarization[23,24], we coapplied the antagonist AIDA along with NBQX and APV. No further reduction of light-evoked currents was observed (Fig. 1k–m), suggesting that iGluRs contribute the major part of SuM-rNSC depolarization.

SuM neurons send sparse projections to the subgranular zone (SGZ) (Fig. 1b), and no robust morphological associations were identified from 3D reconstruction on type 2 progenitors (Fig. 1n). In addition, no light-evoked glutamatergic currents were detected in type 2 progenitors in artificial cerebrospinal fluid (ACSF) (Fig. 1o,p), or in the presence of 4-aminopyridine (4-AP) (Fig. 1p), a voltage-gated potassium channel blocker that increases presynaptic release. This is in sharp contrast to highly responsive rNSCs upon stimulation of SuM-DG projections (Fig. 1q). Together, these results suggest that SuM-DG glutamatergic inputs selectively act on rNSCs, but not on type 2 progenitors.

Stimulation of SuM-DG projections promotes rNSC activation through SuM glutamate transmission. Since we recently established that neural circuit-induced rNSC depolarization is associated with rNSC activation[23,24], we next determined whether rNSC depolarization induced by SuM-DG circuit activation correlates with increased rNSC activation. AAV-DIO-mCherry or AAV-DIO-ChR2-mCherry was delivered to the lateral SuM of Vgat-Cre mice, and patterned blue light illumination was applied above the DG (Extended Data Fig. 1c). As a result, optogenetic activation of SuM-DG projections significantly increased densities of 5-ethynyl-2'-deoxyuridine (EdU)$^+$Nestin$^+$ proliferating rNSCs (Extended Data Fig. 1d–g), EdU$^+$ proliferating progeny (Extended Data Fig. 1h) and EdU$^+$Doublecortin (DCX)$^+$ proliferating neuroblasts (Extended Data Fig. 1i), without altering the densities of Nestin$^+$ rNSCs and DCX$^+$ cells (Extended Data Fig. 1j,k), as compared with controls. These results suggest that stimulation of SuM-DG circuit activity is sufficient to activate rNSCs and increase proliferating neural progenitors/neuroblasts.

Because electrophysiological results demonstrated that SuM-DG circuit activation induces rNSC depolarization, we wondered whether SuM glutamate or GABA might induce neurogenic proliferation of rNSCs. To address this, AAV-DIO-ChR2, along with AAV-expressing short-hairpin RNA against Vglut2 or Vgat, was delivered into the SuM of Vgat-Cre mice (Fig. 1r). The use of Vgat-Cre mice for reliable labeling of SuM neurons has previously been reported[25,35]. In addition, the knockdown efficiency of shVglut2 or shVgat in reducing SuM glutamate or GABA transmission in mature GCs has been validated by slice electrophysiology[25]. As a result of optostimulation of SuM-DG projections, we found increased densities of EdU$^+$/Nestin$^+$ rNSCs, EdU$^+$

Fig. 1 | Activation of SuM-DG projections excites rNSCs through glutamate transmission. a, Diagram of anterograde tracing of SuM-DG projections in Nestin-GFP mice. **b**, Representative SuM projections in the granule cell layer (GCL) of the DG. Scale bar, 100 μm. **c**, Bushy heads of Nestin-GFP$^+$ cells surrounded by SuM-DG projections. Scale bar, 50 μm. **d**, 3D reconstruction of SuM-DG projections, which were closely associated with bushy heads (**i** and **ii**) and soma (**iii**) of nestin-GFP cells. S, soma; yellow arrowheads indicated associations. Scale bars, 20 μm (main image) and 2 μm (insets). **e**, Diagram of ex vivo functional mapping of SuM-DG projections in Nestin-GFP mice. **f**, Biocytin staining of a typical GFP$^+$ rNSC after whole-cell patch-clamp recording. Scale bar, 20 μm. **g**,**h**, Representative traces showing that blue light pulses induced inward currents (**g**) under voltage-clamp mode and depolarizations (**h**) under current-clamp mode in GFP$^+$ rNSCs (potassium-gluconate (GK)-based pipette solution). **i**, Representative traces showing that light-evoked inward currents in GFP$^+$ rNSCs were not affected by bath-applied $GABA_A$ receptor antagonist BIC. Vh, holding potential. **j**, Quantification of light-evoked currents in ACSF or BIC. Data are represented as mean ± s.e.m. $n = 6$ cells, two-sided paired t-test, $P = 0.5405$. **k**, Sample traces of light-evoked inward currents in GFP$^+$ rNSCs before and after application of antagonists iGluR NMDA (APV) + AMPA (NBQX), and mGluR I (AIDA). **l**, Quantification of light-evoked currents under pharmacological conditions shown in **k**. $n = 15$ cells for ACSF and AMPA + APV combination, $n = 9$ cells for AMPA + APV + NBQX combination, one-way ANOVA, $F_{2,36} = 10.18$, $P = 0.0003$. **m**, Summary of the experiments in **k** showing the amplitude of current normalized to ACSF. **n**, Representative image showing SuM projections in the SGZ. Few SuM-DG projections were found in the SGZ (**n**1) and no associations with the intermediate progenitor cell (**n**2). Pink arrowhead indicates the intermediate progenitor cell. Scale bars, 20 μm in **n** and **n**1, 5 μm in **n**2. **o**, Biocytin-labeled GFP$^+$ progenitor cell in the SGZ after whole-cell patch-clamp recording. Scale bar, 20 μm. **p**, Representative traces from voltage-clamp recordings in a GFP$^+$ progenitor cell following optical activation of SuM-DG projections in ACSF (upper) or 4-AP (lower) bath application. **q**, Proportion of rNSCs and intermediate progenitor cells functionally connected or unconnected to SuM. Fisher's exact test, $P < 0.0001$, from 18 mice. **r**, Diagram and stimulation paradigm for in vivo optogenetic activation of SuM^{Vgat}-DG projections with shVglut2 or shVgat expression in the SuM. **s**–**u**, Density of EdU$^+$/Nestin$^+$ (**s**), EdU$^+$ (**t**) and EdU$^+$/DCX$^+$ (**u**) in DG after optogenetic stimulation. $n = 7$, 8 and 6 mice in groups ChR2, shVglut2/ChR2 and shVgat/ChR2, respectively. One-way ANOVA; **s**, $F_{2,18} = 12.38$, $P = 0.0004$; **t**, $F_{2,18} = 9.338$, $P = 0.0017$; **u**, $F_{2,18} = 31.67$, $P < 0.0001$, followed by Tukey's post hoc test. NS, not significant.

proliferating progeny and EdU$^+$DCX$^+$ proliferating neuroblasts, which were abolished by expression of shVglut2 (but not by shVgat) in SuM neurons (Fig. 1s–u and Extended Data Fig. 1l–n). These results suggest that SuM glutamate (but not GABA) transmission induced activation of rNSCs and production of proliferating newborn progeny.

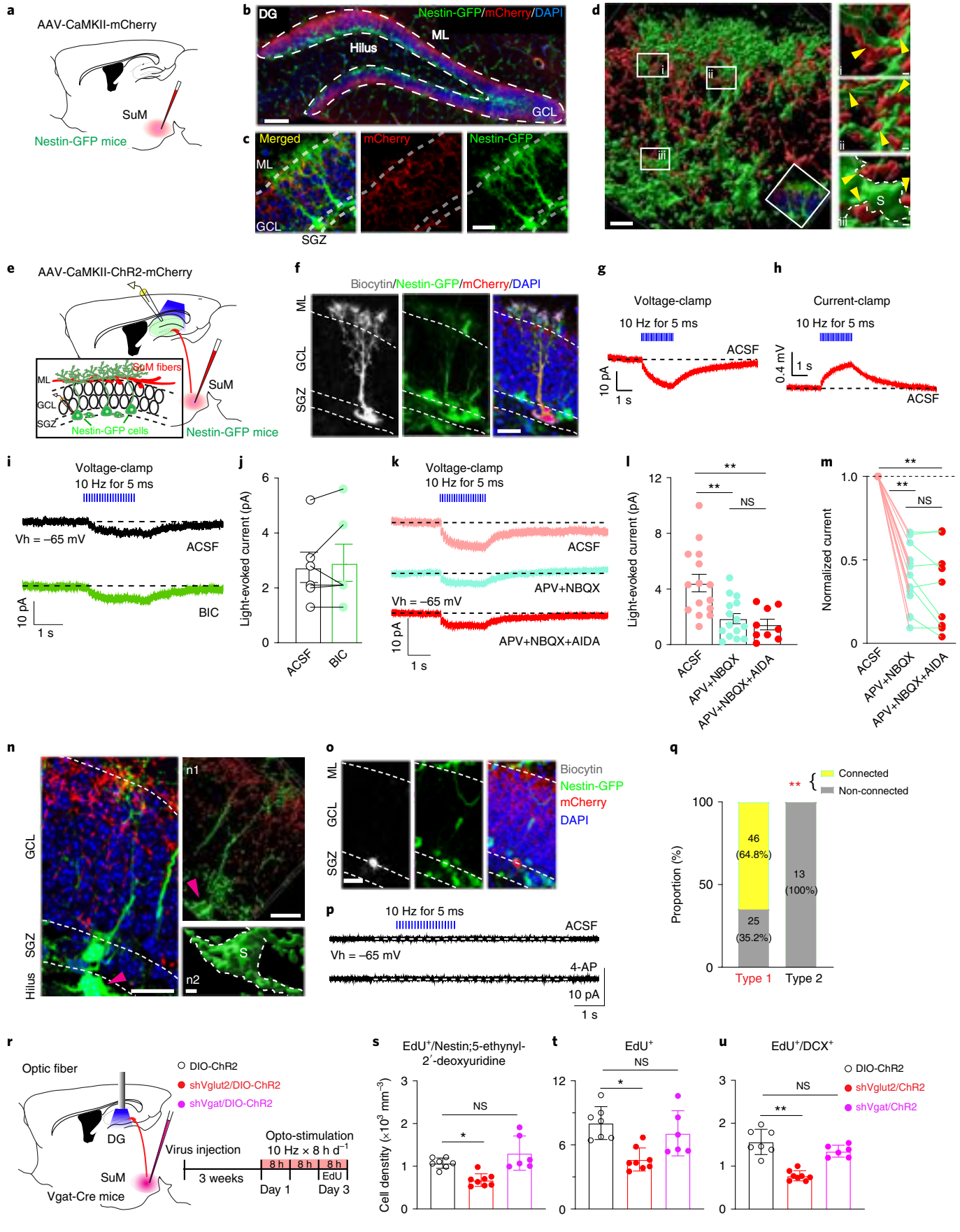

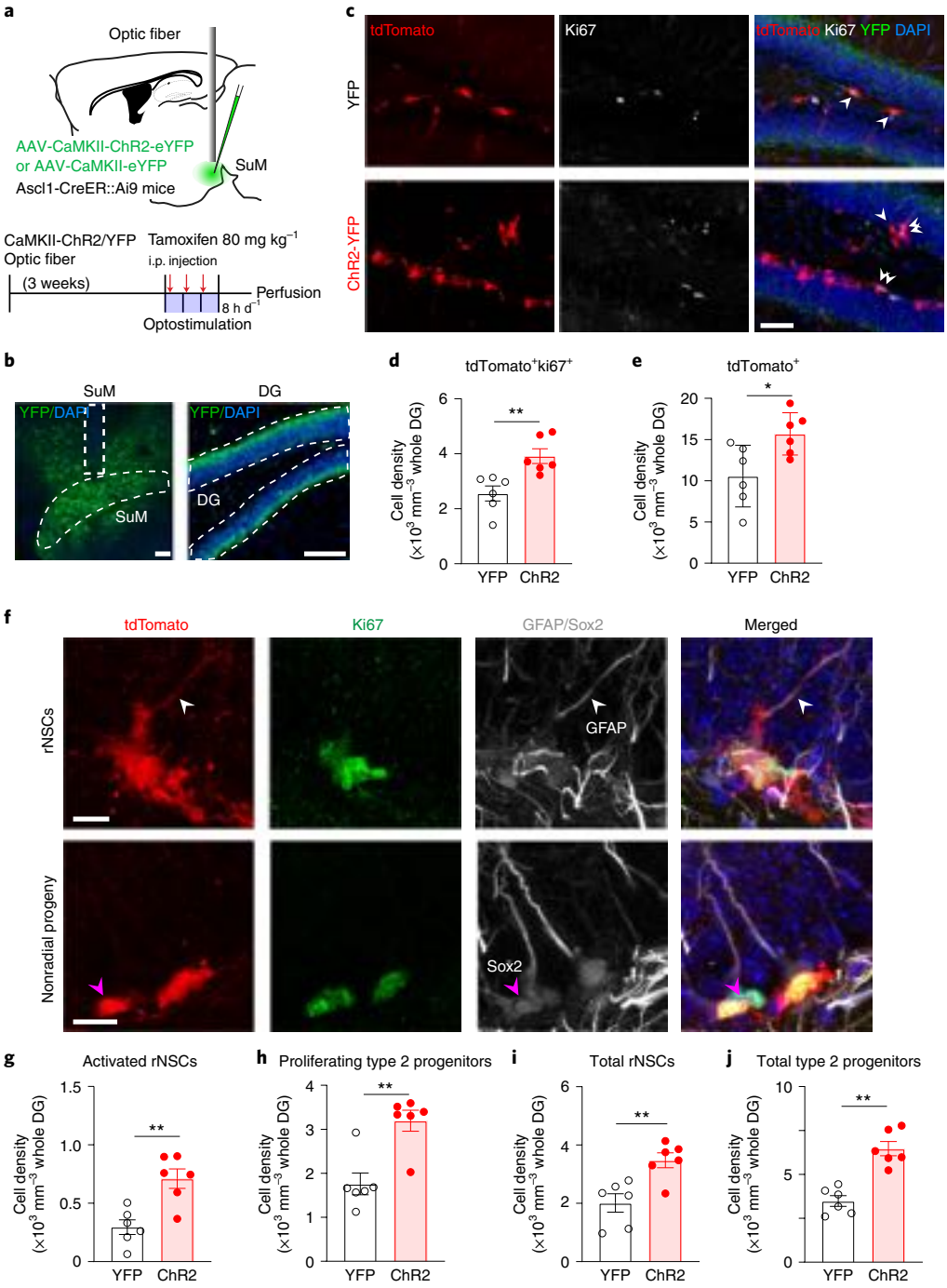

Fig. 2 | Stimulation of SuM neurons promotes production of rNSCs and neural progenitors. a, Diagram and stimulation paradigm for optogenetic stimulation of SuM neurons in Ascl1-Ai9 mice. **b**, Sample images of ChR2-YFP expression in SuM neurons and terminals in the DG. Scale bars, 100 µm. Fiber implantation location is indicated by dotted lines. **c**, Sample images of tdTomato$^+$ and Ki67$^+$ cells in the DG after optogenetic stimulation of SuM neurons. White arrowheads indicated tdTomato$^+$Ki67$^+$ cells. Scale bar, 50 µm. **d**,**e**, Density of tdTomato$^+$/Ki67$^+$ (**d**) and tdTomato$^+$ (**e**) cells in the DG after optogenetic stimulation of SuM neurons. $n=6$ mice per group, two-sided unpaired *t*-test; **d**, $P=0.0053$, **e**, $P=0.02$. **f**, Representative identification of proliferative/nonproliferative rNSCs and nonradial progeny. Top, rNSCs were identified as tdTomato$^+$ cells containing a GFAP$^+$ radial process (white arrowheads). Activated status was determined by the presence of Ki67. Bottom, nonradial progeny were counted as tdTomato$^+$Sox2$^+$ cells without a GFAP$^+$ radial process (pink arrowheads). Proliferative status was determined by the presence of Ki67. Scale bars, 20 µm. **g**–**j**, Density of activated rNSCs (**g**), proliferating type 2 progenitors (**h**), total rNSCs (**i**) and total type 2 progenitors (**j**) in the DG after optogenetic stimulation of SuM neurons. $n=6$ mice per group, two-sided unpaired *t*-test; **g**, $P=0.0026$; **h**, $P=0.0002$; **i**, $P=0.0048$; **j**, $P=0.0019$..

Stimulation of SuM neurons during early neurogenesis promotes production of rNSCs and neural progenitors. To study the cumulative neurogenic effects mediated by sustained circuit manipulation, we combined SuM stimulation with indelible lineage tracing of adult neural precursors by crossing mice expressing tamoxifen-inducible Cre recombinase under the control of the

endogenous Achaete-scute homolog 1 promoter (Ascl1CreER)[36] to a floxed tdTomato reporter line (Ai9) to label rNSCs and type 2 neural progenitors (Ascl1-Ai9 mice). Of note, rNSCs are highly heterogeneous[37,38] and Ascl1$^+$ rNSCs are thought to represent the 'neurogenic' rNSC subpopulation[36,39–41]. To achieve the broad circuit effects on neurogenesis and minimize surgical injury within the DG, we implanted a single optogenetic fiber above the SuM for optogenetic stimulation (SuM neurons project to the dorsoventral axis of bilateral DG), as opposed to bilateral implantation of multiple optical fibers to cover dorsoventral SuM-DG projections.

We first examined the effects of optogenetic activation of SuM neurons on rNSCs and type 2 neural progenitors. Specifically, we injected AAV-CaMKII-ChR2-YFP or AAV-CaMKII-YFP into the SuM of Ascl1-Ai9 mice, followed by tamoxifen induction for three consecutive days (one injection daily) along with optostimulation of SuM neurons (Fig. 2a,b). We confirmed that optostimulation induced c-Fos expression in SuM neurons (Extended Data Fig. 2a,b). Optostimulation significantly increased the densities of Ki67$^+$tdTomato$^+$ proliferating cells and overall tdTomato$^+$ cells (Fig. 2c–e). Densities of activated rNSCs (GFAP$^+$Ki67$^+$ tdTomato$^+$ with radial morphology), proliferating type 2 progenitors (Sox2$^+$Ki67$^+$tdTomato$^+$ with horizontal morphology), as well as total tdTomato$^+$ rNSCs and type 2 progenitors, were also increased (Fig. 2f–j and Extended Data Fig. 2c). These results suggest that stimulation of SuM neurons promotes production of rNSCs and progenitors, potentially through increased symmetric self-renewal and asymmetric neurogenic proliferation of rNSCs.

For validation, a chemogenetic approach was used to activate SuM neurons by injection of AAVs expressing excitatory designer receptors exclusively activated by designer drugs (DREADDs)—AAV-DIO-hM3Dq-mCherry or mCherry (AAV-DIO-mCherry)—into the SuM of Vgat-Cre mice (Extended Data Fig. 3a,b). Consistent with our results from optostimulation of SuM neurons, chemogenetic activation of SuM neurons increased densities of both proliferating rNSCs and progenitors (Extended Data Fig. 3c–h).

Because either opto- or chemostimulation can induce SuM neuronal activity at nonphysiological levels, a loss-of-function approach was used to address whether SuM activity is required for mediation of hippocampal neurogenesis (Extended Data Fig. 3a). AAVs expressing inhibitory DREADDs (AAV-DIO-hM4Di-mCherry) or mCherry (AAV-DIO-mCherry) were delivered to the SuM of Vgat-Cre mice (Extended Data Fig. 3a). As a result of chemogenetic inhibition of SuM neurons, densities of EdU$^+$Nestin$^+$ rNSCs, EdU$^+$ proliferating progeny and EdU$^+$DCX$^+$ proliferating neuroblasts were significantly decreased (Extended Data Fig. 3i–n) as compared with controls. These results suggest that activity of SuM neurons is required for early hippocampal neurogenesis.

SuM GABA transmission is required for differentiation of neural progenitors. A question raised is whether SuM activity-induced increase in newborn progeny can be maintained into later neurogenesis stages. To address this, we optogenetically stimulated SuM neurons in Ascl1-Ai9 mice as before and examined the density of tdTomato$^+$ ABNs at 6 weeks post tamoxifen induction. At this time point, the density of tdTomato$^+$ ABNs was unchanged (Extended Data Fig. 2d–f), suggesting that additional stimuli beyond initial neurogenesis stages are required to support integration of SuM activity-induced progeny. Therefore, we wondered whether SuM inputs act on other neurogenesis stages. Newborn progenitors/neuroblasts derived from rNSCs are known to first receive depolarizing GABAergic inputs, followed by glutamatergic inputs[42]. To address whether these newborn progeny receive direct SuM-mediated GABA inputs, we recorded tdTomato$^+$ newborn progeny with horizontal morphology from Ascl1-Ai9 mice 9–12 days post tamoxifen induction (dpi) upon optostimulation of SuM-DG projections (Extended Data Fig. 4a). GABA currents were isolated by high-chloride internal solution in the presence of iGluR blockers. Of note, tdTomato$^+$ cells exhibited high input resistance characteristic of the cell stage when GABA is depolarizing[42] (Extended Data Fig. 4c,h). No light-evoked GABAergic currents were detected in these cells, even in the presence of 4-AP to increase presynaptic release, or of vigabatrin to boost synaptic GABA levels (Extended Data Fig. 4b–e). These results suggest there are no direct SuM GABAergic inputs on these cell stages, which aligns with the morphological evidence showing sparse SuM projections onto neural progenitors (Fig. 1n).

It has been shown that soma-targeting DG interneurons receive predominant SuM GABAergic inputs[29] while newborn progeny receive inputs from DG interneurons[21]. Therefore, it is possible that SuM GABAergic inputs play an indirect role in regulation of newborn progeny. We decided to directly address the in vivo role of SuM GABA in regulation of these cells by knocking down SuM GABA transmission. AAV-CaMKII-YFP or AAV-CaMKII-ChR2 was delivered to the SuM of Ascl1-Ai9 mice with or without AAV-shVgat (Fig. 3a). AAV-injected mice were induced with tamoxifen for 2 days and received patterned SuM stimulation lasting 16 days (Fig. 3a). Total tdTomato$^+$ and tdTomato$^+$DCX$^+$ cells were increased after optogenetic activation of SuM neurons (Fig. 3b). Knockdown of Vgat in SuM neurons did not alter the increase in total tdTomato$^+$ density (Fig. 3c) but reduced tdTomato$^+$DCX$^+$ cell density (Fig. 3d). Moreover, the density of DCX$^-$tdTomato$^+$ cells in ChR2-shVgat mice was significantly increased as compared with ChR2 mice (Fig. 3e). These results suggest that reduction of SuM GABAergic inputs impairs the differentiation of neural progenitors, leading to accumulation of DCX$^-$ neural progenitors and reduced production of DCX$^+$ neuroblasts/immature neurons, potentially through an indirect mechanism mediated by local interneurons.

Fig. 3 | SuM GABA transmission regulates neural progenitors and early-stage immature neurons. a, Diagram and paradigm of optogenetic stimulation of SuM-DG projections expressing shVgat in the SuM of Ascl1-Ai9 mice. **b**, Sample images of tdTomato$^+$ and DCX$^+$ staining of Ascl1-Ai9 mice at 16 dpi. TdTomato$^+$DCX$^+$ and tdTomato$^+$DCX$^-$ cells are indicated by closed and open arrowheads, respectively. Scale bar, 50 μm. **c**–**e**, Density of tdTomato$^+$ (**c**), DCX$^+$tdTomato$^+$ (**d**) and DCX$^-$tdTomato$^+$ (**e**) cells after 16-day optogenetic stimulation of SuM-DG projections in Ascl1-Ai9 mice. $n = 5$ mice for each group. One-way ANOVA; **c**, $F_{2,12} = 25.25$, $P < 0.0001$; **d**, $F_{2,12} = 30.2$, $P < 0.0001$; **e**, $F_{2,12} = 31.70$, $P < 0.0001$, followed by Tukey's post hoc test. **f**, Experimental scheme for slice electrophysiological recording of immature neurons (12 dpi) for ex vivo optogenetic stimulation of SuM-DG projections in Ascl1-Ai9 mice. **g**, Confocal images of a biocytin-labeled tdTomato$^+$DCX$^+$ cell at 12 dpi after whole-cell patch-clamp recording. Scale bar, 20 μm. **h**, Representative traces showing that optogenetic activation of SuM-DG projections induces inward currents (top) in a 12 dpi immature neuron (KCl-based pipette solution), which was blocked by the $GABA_A$R antagonist BIC (bottom); **h**1, enlarged traces from the boxed region in ACSF. Individual traces (gray) were shown, with the average in red. **i**, An immature neuron at 12 dpi received mixed synaptic and tonic GABAergic currents from SuM neurons (top, in ACSF; bottom, in $GABA_A$R antagonist BIC), KCl-based pipette solution. **j**, Diagram of in vivo optogenetic stimulation of SuM neurons for 16 days in Ascl1-Ai9 mice. **k**, Sample images of an immature tdTomato$^+$ neuron at 16 dpi for morphology analysis. Scale bar, 20 μm. **l**, Confocal overview of tdTomato$^+$ cells and ChR2-YFP terminals from SuM neurons in the DG at 16 dpi. Scale bar, 200 μm. **m**, Morphology of individual tdTomato$^+$ cells at 16 dpi following optogenetic stimulation. Scale bar, 10 μm. **n**–**p**, Sholl analysis (**n**), dendrite length (**o**) and total dendrite branches (**p**) of tdTomato$^+$ cells at 16 dpi. $n = 54$ cells for YFP group and $n = 53$ cells for ChR2 group, $^{**}P < 0.0001$ by two-sided unpaired *t*-test. Mol, molecular layer.

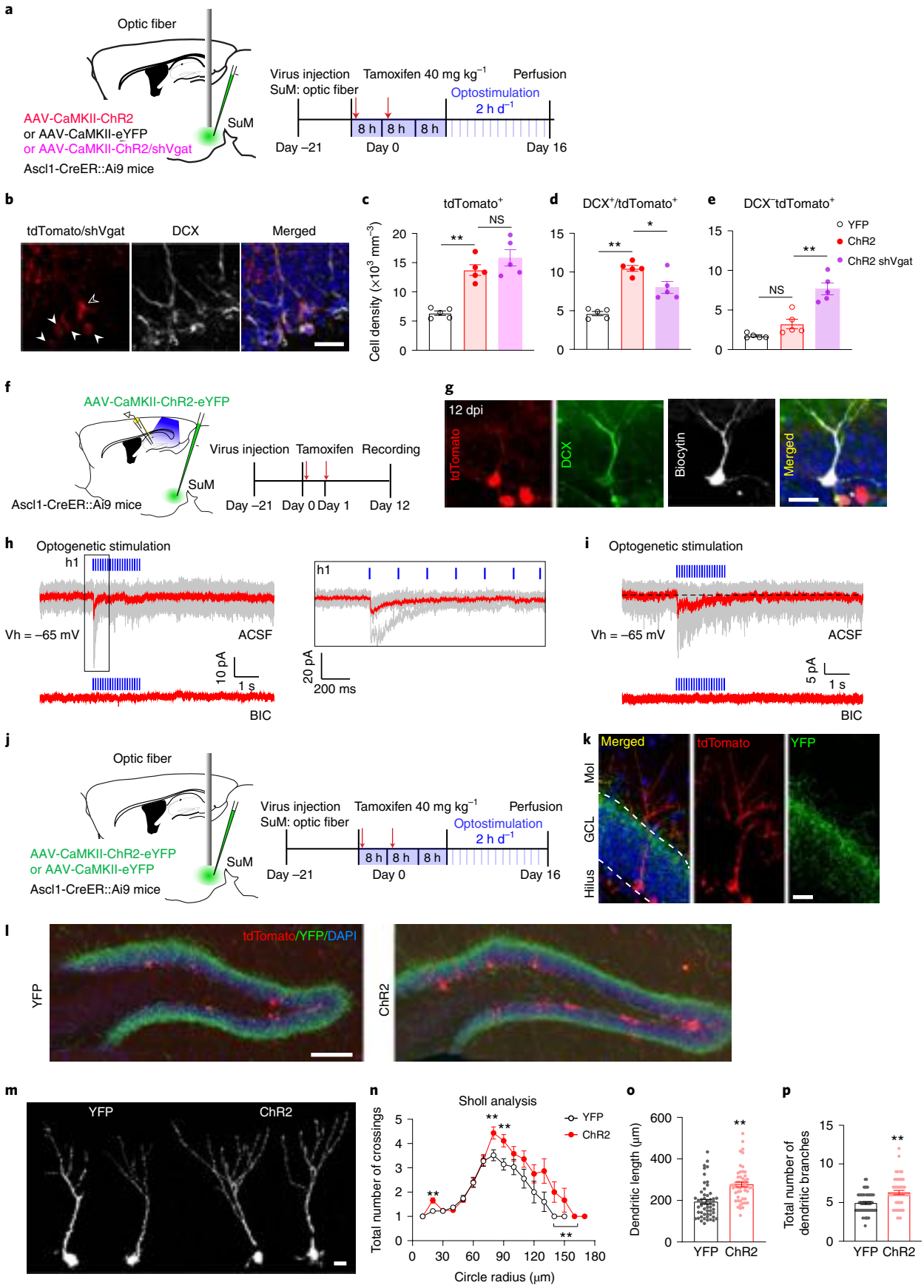
a
Optic fiber
AAV-CaMKII-ChR2
or AAV-CaMKII-eYFP
or AAV-CaMKII-ChR2/shVgat
Ascl1-CreER::Ai9 mice
SuM
Virus injection
SuM: optic fiber
Tamoxifen 40 mg kg−1
Perfusion
Optostimulation
2 h d−1
8 h 8 h 8 h
Day –21
Day 0
Day 16
b
tdTomato/shVgat
DCX
Merged
c
tdTomato+
Cell density (×10³ mm⁻³)
NS
**
d
DCX+/tdTomato+
*
e
DCX−tdTomato+
YFP
ChR2
ChR2 shVgat
f
AAV-CaMKII-ChR2-eYFP
Ascl1-CreER::Ai9 mice
SuM
Virus injection
Tamoxifen
Recording
Day –21
Day 0
Day 1
Day 12
g
12 dpi
tdTomato
DCX
Biocytin
Merged
h
Optogenetic stimulation
h1
Vh = –65 mV
ACSF
10 pA
1 s
BIC
20 pA
200 ms
i
Optogenetic stimulation
Vh = –65 mV
ACSF
5 pA
1 s
BIC
j
Optic fiber
AAV-CaMKII-ChR2-eYFP
or AAV-CaMKII-eYFP
Ascl1-CreER::Ai9 mice
SuM
Virus injection
SuM: optic fiber
Tamoxifen 40 mg kg−1
Perfusion
Optostimulation
2 h d−1
8 h 8 h 8 h
Day –21
Day 0
Day 16
k
Merged
tdTomato
YFP
Mol
GCL
Hilus
l
tdTomato/YFP/DAPI
YFP
ChR2
m
YFP
ChR2
n
Sholl analysis
Total number of crossings
Circle radius (μm)
YFP
ChR2
o
Dendritic length (μm)
YFP
ChR2
p
Total number of dendritic branches
YFP
ChR2

SuM neurons provide direct GABAergic inputs to regulate dendritic development of adult-born immature neurons. Next we sought to address whether adult-born immature neurons receive direct SuM GABAergic inputs, by recording light-evoked currents in tdTomato$^+$ cells exhibiting immature neuron morphology (Fig. 3f–i and Extended Data Fig. 4f–j). Optogenetic activation of SuM-DG projections induced light-evoked responses in 35% of tdTomato$^+$ immature neurons at 12 dpi, but not at 9 dpi (Extended Data Fig. 4j). Importantly, light-evoked responses were abolished in the presence of BIC (Fig. 3h,i), confirming GABAergic SuM inputs. The responses were heterogeneous, with some in tdTomato$^+$ cells showing typical synaptic responses (Fig. 3h) and others showing mixed synaptic/tonic responses (Fig. 3i). Importantly, all responses exhibited short delay times of around 4.5 ms, typically considered as monosynaptic connections. Conversely, no light-evoked glutamatergic currents could be detected in tdTomato$^+$ immature neurons at 12 dpi (0/14 cells) (Extended Data Fig. 4f–j). These results suggest that immature neurons receive monosynaptic GABAergic (but not glutamatergic) inputs from SuM neurons as early as 12 dpi.

Depolarization of GABA signaling can also regulate dendritic development of immature neurons[42,43]. Examination of immature tdTomato$^+$ neurons following 16-day optogenetic activation of SuM neurons in Ascl1-Ai9 mice revealed a significant increase in total dendritic length, branch number and complexity (Fig. 3j–p). Given that adult-born immature neurons do not receive SuM glutamatergic inputs at this stage (Extended Data Fig. 4f–j), these results suggest that SuM GABAergic inputs promote dendritic development of immature neurons.

Chronic patterned stimulation of SuM neurons promotes the production and maturation of ABNs. Four- to 6-week-old ABNs are known to possess unique physiological properties with heightened plasticity, capable of modulating hippocampus-dependent behaviors[5,8]. Slice recording from tdTomato$^+$ cells in Ascl1-Ai9 mice at 32 dpi demonstrated electrophysiological properties characteristic of immature neurons as compared with mature GCs, including lower membrane capacity, higher input resistance, greater depolarized membrane potential and higher intrinsic excitability (Extended Data Fig. 5a–d). Importantly, these electrophysiological properties are highly consistent with those reported for ABNs during the critical period of enhanced plasticity[4–9].

Since mature GCs receive dual SuM GABAergic/glutamatergic inputs[25], we wondered whether ABNs also receive dual inputs. Recordings were made of light-evoked GABAergic and glutamatergic postsynaptic currents (PSCs) in tdTomato$^+$ ABNs at 5 mV (close to the reversal potential of glutamatergic PSCs to isolate GABAergic PSCs) and −60 mV (close to the reversal potential of GABAergic PSCs to isolate glutamatergic PSCs), to detect SuM input components (Fig. 4a,b). Surprisingly, only 27% (3/11) of recorded tdTomato$^+$ cells exhibited dual inputs. In addition, 18% (2/11) exhibited sole glutamatergic inputs and 55% (6/11) exhibited sole GABAergic inputs (Fig. 4b and Extended Data Fig. 5k). Compared with mature GCs, 32 dpi ABNs exhibited immature features, including longer delay time in response to optostimulation of SuM-DG projections and lower mean amplitude in light-evoked PSCs (Extended Data Fig. 5e–k). Next we sought to address when these ABNs start to receive SuM glutamatergic inputs, by recording tdTomato$^+$ cells at 22, 26 and 28 dpi. As a result, tdTomato$^+$ cells at 22 and 26 dpi exhibited only light-evoked SuM GABAergic inputs (Extended Data Fig. 5l,m); light-evoked SuM glutamatergic inputs were found in only a small portion of tdTomato$^+$ cells (1/8) starting at 28 dpi (Fig. 4c). Together, these results suggest that adult-born cells during development receive either SuM glutamate (rNSCs) or GABA inputs (early/midstage immature neurons), and that dual SuM glutamate/GABA or sole SuM glutamate inputs appear only in late-stage immature neurons.

To study the long-term effects of SuM stimulation on ABNs, AAV-injected Ascl1-Ai9 mice were induced with tamoxifen for 3 days, along with chronic SuM stimulation following a 32-day patterned light paradigm (Fig. 4d). This paradigm was designed to maximize production of rNSCs and progenitors during initial stages and provide sustained stimuli critical for integration and maturation of immature neurons at later stages. Tissue integrity was examined in SuM after chronic optostimulation by Iba1 and GFAP immunohistology, and no significant differences in expression were detected after 32-day light exposure (Extended Data Fig. 5n). Chronic stimulation of SuM neurons significantly increased the densities of tdTomato$^+$ and NeuN$^+$tdTomato$^+$ neurons in ChR2-Ascl1-Ai9 mice, as compared with controls (Fig. 4d–o). Importantly, SuM stimulation increased the density of DCX$^-$NeuN$^+$tdTomato$^+$ cells (Fig. 4k) and decreased the percentage of DCX$^+$tdTomato$^+$ cells (Fig. 4m), suggesting enhanced maturation of ABNs. Furthermore, ChR2-Ascl1-Ai9 mice exhibited significantly higher spine density in ABNs as compared with control mice (Fig. 4p,q).

Activity of SuM-modified ABNs further modulates memory performance. Several studies have reported that ABN activity is critical for memory[7,8,44,45] and emotional behaviors[46–48]. To establish the behavioral contribution of ABN activity, we expressed DREADDs[49] in ABNs by crossing floxed hM3Dq or hM4Di mice[50] with Ascl1CreER mice to generate double-transgenic mice (Ascl1-hM3Dq or Ascl1-hM4Di) (Extended Data Fig. 6a,b,j,k); hM3Dq and hM4Di floxed mice were used as controls. C-Fos staining (Extended Data Fig. 7a,d,e) and slice electrophysiology (Extended Data Fig. 7c,f) confirmed activation or inhibition of Ascl1-hM3Dq/hM4Di cells by clozapine-*N*-oxide (CNO) induction. Whole-brain analysis of hM3/hM4 molecular tags confirmed restricted expression to the SGZ/DG and olfactory bulb (OB) only (Extended Data Fig. 7i,j). Since SuM neurons project to the DG (but not to the OB) and OB neurons are not involved in hippocampus-dependent behaviors, the causal

Fig. 4 | SuM neurons promote maturation and dendritic spine development of late-stage adult-born immature neurons. a, Electrophysiological recording scheme of late-stage immature neurons for optogenetic stimulation of SuM-DG projections in slices from Ascl1-Ai9 mice at 28/32 dpi. **b**, Sample traces showing tdTomato$^+$ cells at 32 dpi receiving glutamate and GABA inputs (left) or glutamate-only inputs (right) upon optogenetic activation of SuM-DG projections (Cs-based pipette solutions). **c**, Sample traces showings tdTomato$^+$ cells at 28 dpi receiving glutamate inputs upon optogenetic activation of SuM-DG projections, which was blocked by the AMPAR antagonist APV and the NMDAR antagonist NBQX (GK-based pipette solution). **d**, Diagram of in vivo optogenetic stimulation of SuM neurons in Ascl1-Ai9 mice for 32 days. **e**, Representative confocal images of tdTomato$^+$ cells after optogenetic stimulation at 32 dpi. Scale bar, 200 µm. **f**, Representative confocal images of tdTomato$^+$DCX$^+$NeuN$^+$ cells in the DG. Solid arrowheads indicate tdTomato$^+$NeuN$^+$ cells, hollow arrowheads indicate tdTomato$^+$DCX$^+$NeuN$^-$ cells. Scale bar, 20 µm. **g**, Quantification of density of tdTomato$^+$ cells after 32-day optogenetic stimulation. $n = 6$ mice per group, $P = 0.0470$ by two-sided unpaired *t*-test. **h**–**k**, Density of tdTomato$^+$ cells that were also NeuN$^+$ (**h**), DCX$^+$ (**i**), NeuN$^+$DCX$^+$ (**j**) or NeuN$^+$DCX$^-$ (**k**) in the DG after 32-day optogenetic stimulation. $n = 6$ mice per group, two-sided unpaired *t*-test; **h**, $P = 0.0103$; **i**, $P = 0.2820$; **j**, $P = 0.0660$; **k**, $P = 0.0055$. **l**–**o**, Percentage (normalized to total tdTomato$^+$ cells) of tdTomato cells that were NeuN$^+$ (**l**), DCX$^+$ (**m**), NeuN$^+$DCX$^+$ (**n**) or NeuN$^+$DCX$^-$ (**o**) after 32-day optogenetic stimulation of SuM neurons. $n = 6$ mice per group; **h**, $P = 0.3831$; **i**, $P = 0.0496$; **j**, $P = 0.1881$; **k**, $P = 0.6194$. **p**,**q**, Sample dendritic segments (**p**) and density quantification (**q**) of dendrite spines on tdTomato$^+$ dendrites after optogenetic stimulation. Scale bar, 1 µm. $n = 4$ mice per group, $P = 0.0192$ by two-sided unpaired *t*-test.

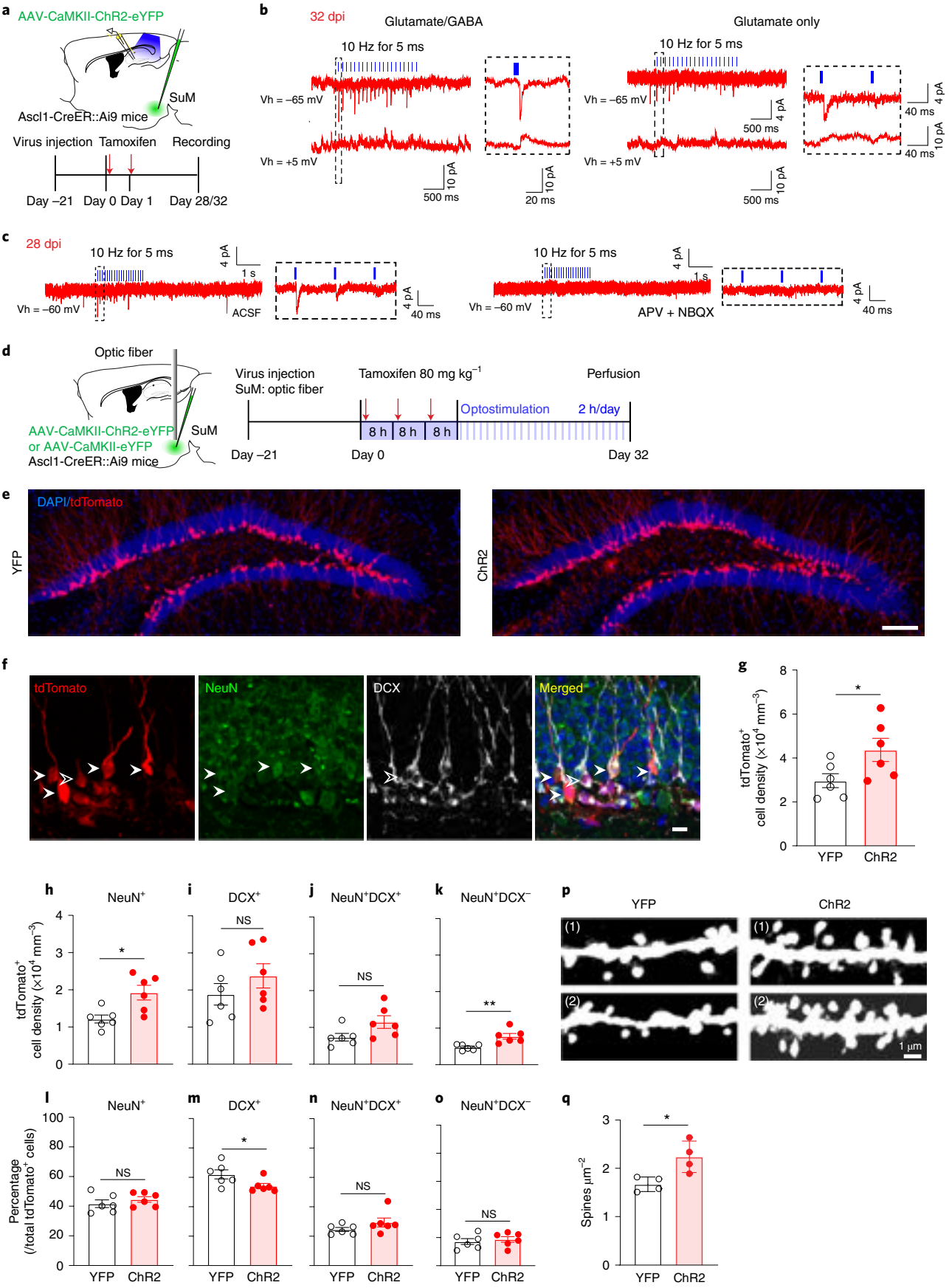
a
AAV-CaMKII-ChR2-eYFP
SuM
Ascl1-CreER::Ai9 mice
Virus injection Tamoxifen Recording
Day –21 Day 0 Day 1 Day 28/32
b
32 dpi
Glutamate/GABA
10 Hz for 5 ms
Vh = –65 mV
Vh = +5 mV
10 pA
500 ms
20 ms
Glutamate only
4 pA
40 ms
c
28 dpi
Vh = –60 mV
ACSF
APV + NBQX
1 s
d
Optic fiber
AAV-CaMKII-ChR2-eYFP
or AAV-CaMKII-eYFP
Virus injection
SuM: optic fiber
Tamoxifen 80 mg kg−1
8 h 8 h 8 h
Optostimulation
2 h/day
Perfusion
Day –21 Day 0 Day 32
e
DAPI/tdTomato
YFP
ChR2
f
tdTomato
NeuN
DCX
Merged
g
tdTomato+ cell density (×10^4 mm−3)
YFP ChR2
h
NeuN+
i
DCX+
j
NeuN+DCX+
k
NeuN+DCX−
NS
l
Percentage (/total tdTomato+ cells)
m
n
o
p
YFP
ChR2
(1)
(2)
1 μm
q
Spines μm−2

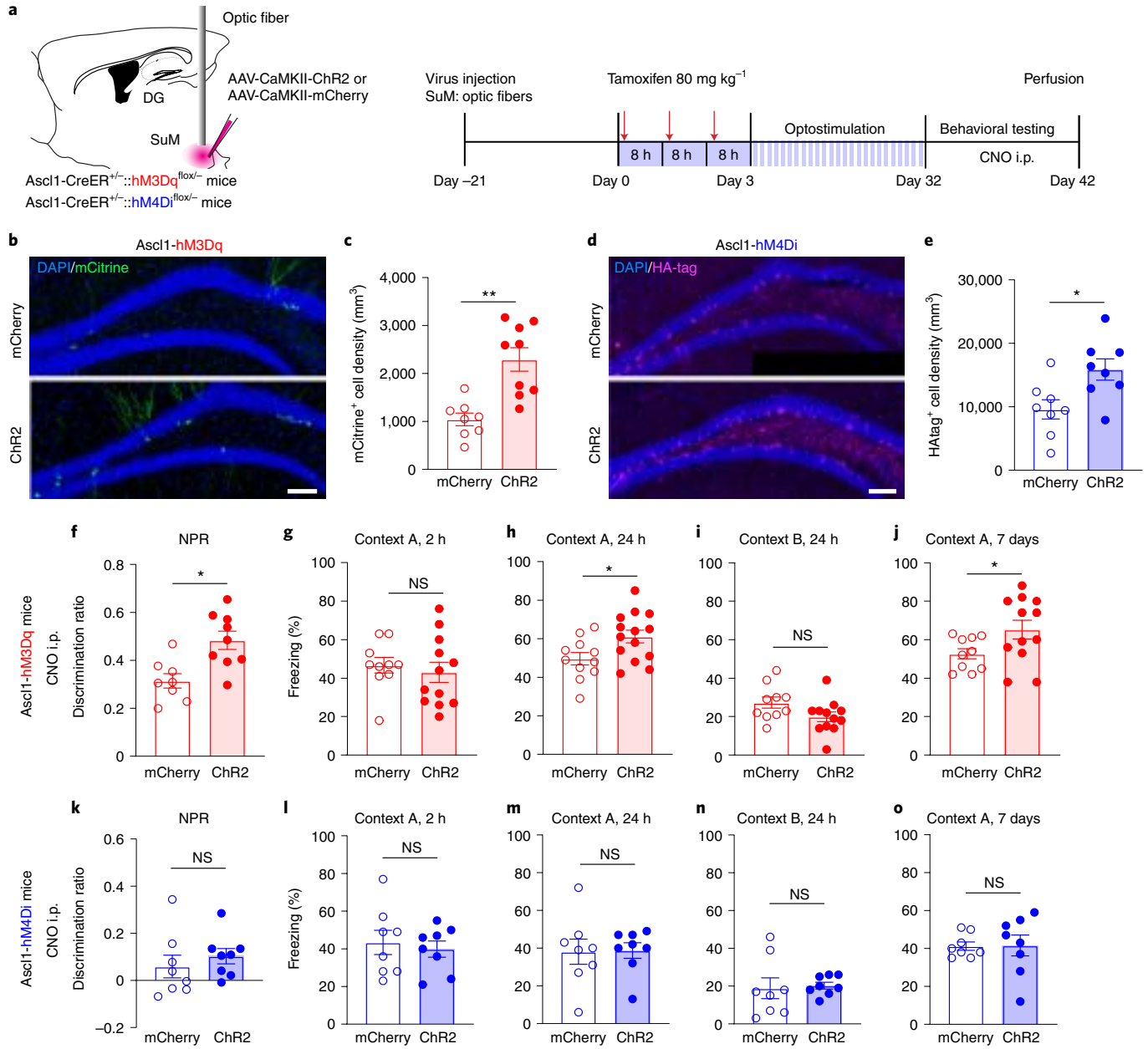

Fig. 5 | Activation of SuM circuit-modified ABNs further improves memory performance. a, Experimental design for behavioral testing during chemogenetic activation or inhibition of ABNs after optogenetic stimulation of SuM neurons for 32 days in Ascl1-hM3Dq or Ascl1-hM4Di mice. **b**,**c**, Sample images showing expression (**b**) and density (**c**) of mCitrine$^+$ hM3Dq cells in the DG of AAV-mCherry- or AAV-ChR2-injected Ascl1-hM3Dq mice after optogenetic stimulation. Scale bars, 100 µm. $n=8$ mice for mCherry group, $n=9$ mice for ChR2 group, $P=0.0006$ by two-sided unpaired *t*-test. **d**,**e**, Sample images showing expression (**d**) and density (**e**) of HA-tag$^+$ hM4Di cells in the DG of AAV-mCherry- or AAV-ChR2-injected Ascl1-hM4Di mice after optogenetic inhibition. Scale bar, 100 µm. $n=8$ mice in each group, $P=0.0184$ by two-sided unpaired *t*-test. **f**, Chemogenetic activation of circuit-modified newborn neurons further enhanced discrimination ratio in the NPR test. $n=8$ mice for mCherry group, $n=9$ mice for ChR2 group. $P=0.0438$ by two-sided unpaired *t*-test. **g**–**j**, Freezing time in context A at 2 h (**g**) and 24 h (**h**), in context B at 24 h (**i**) and in context A at 7 days (**j**) after chemogenetic activation of SuM circuit-modified or unmodified newborn neurons. $n=8$ mice for mCherry group, $n=9$ mice for ChR2 group, two-sided unpaired *t*-test; **h**, $P=0.8273$; **i**, $P=0.0228$; **j**, $P=0.1812$; **k**, $P=0.0255$. **k**, Chemogenetic inhibition of circuit-modified newborn neurons did not change discrimination ratio in the NPR test. $n=8$ mice for each group, $P=0.4615$ by two-sided unpaired *t*-test. **l**–**o**. Freezing time in context A at 2 h (**l**) and 24 h (**m**), in context B at 24 h (**n**) and in context A at 7 days (**o**) after chemogenetic inhibition of SuM circuit-modified and unmodified newborn neurons. $n=8$ mice per group, two-sided unpaired *t*-test; **l**, $P=0.6585$; **m**, $P=0.9374$; **n**, $P=0.8168$; **o**, $P=0.6433$.

role of SuM-modified ABNs in behavioral modulation can be established using these mouse lines.

We first examined the effects of acute chemogenetic manipulation of ABNs (32 dpi) on memory performance (Extended Data Fig. 6a). Ascl1-hM3Dq/hM4Di or hM3Dq/hM4Di mice were subjected to two DG-dependent tasks, including novel place recognition (NPR) (Extended Data Fig. 6c) and contextual fear conditioning (CFC) (Extended Data Fig. 6d). Chemogenetic activation of ABNs significantly increased discrimination ratio in the NPR test (Extended Data Fig. 6e). In addition, freezing time was increased in context A

(but not in context B) at 24 h and 7 days (but not at 2 h) in the CFC test (Extended Data Fig. 6f–i). These results suggest that activation of ABNs improves both spatial and contextual memory retrieval. By contrast, chemogenetic inhibition of ABNs in Ascl1-hM4Di mice significantly decreased discrimination ratio in the NPR test (Extended Data Fig. 6l) while freezing time in the CFC test was unchanged (Extended Data Fig. 6m–p). There was no significant difference in locomotion of these mice during ABN activity manipulation (Extended Data Fig. 7g,h). Taken together, these findings suggest that the activity of ABNs is both sufficient and necessary for regulation of spatial memory retrieval. Interestingly, the activity of ABNs is sufficient (but not necessary) for contextual memory only, suggesting that the activity of ABNs may play differential roles in regulation of distinct forms of memory.

These findings raised the important question as to whether SuM-modified ABNs could further modulate memory performance. To address this, we delivered AAV-CaMKII-ChR2-mCherry or AAV-CaMKII-mCherry into the SuM of Ascl1-hM3Dq/hM4Di mice to generate SuM-modified ABNs (ChR2-Ascl1-hM3Dq/hM4Di mice) or noncircuit-modified ABNs (control). Both ChR2 and control mice received the same light paradigm. Similar to Ascl1-Ai9 mice, increased densities of mCitrine$^+$hM3Dq$^+$ cells in Ascl1-hM3Dq (Fig. 5b,c), and of HA$^+$hM4Di$^+$ cells in Ascl1-hM4Di mice (Fig. 5d,e), were found following chronic SuM activation.

NPR and CFC tests were then performed to address whether activity of SuM-modified ABNs could further modulate memory performance. Behavioral tests were performed 1 day after optostimulation of SuM, to rule out potential acute circuit effects immediately following SuM stimulation. Chemogenetic activation of SuM-modified ABNs in ChR2-Ascl1-hM3Dq mice significantly increased discrimination ratio in the NPR test (Fig. 5f) as compared with control mice following chemogenetic activation of ABNs without SuM stimulation. Moreover, such manipulation significantly increased freezing time in context A at 24 h and 7 days (but not at 2 h) after foot shocks during the CFC test (Fig. 5g–j). These results suggest that activation of SuM-modified ABNs is sufficient to further improve both spatial and contextual memory retrieval. By contrast, chemogenetic inhibition of SuM-modified ABNs in ChR2-Ascl1-hM4Di mice did not further impair memory retrieval in either test (Fig. 5k–o), suggesting that activity of SuM-modified ABNs is not required for further modulation of memory retrieval. Taken together, these results suggest that activity of SuM-modified ABNs is critical for memory retrieval, because activation of SuM-modified ABNs further improves memory performance.

Activity of SuM-modified ABNs further modulates anxiety-like behavior. To address the role of SuM-modified ABNs in regulation of emotion processing, open field, zero maze, and forced swimming tests were performed in Ascl1-hM3Dq/hM4Di and control-hM3Dq/hM4Di mice (Fig. 6a). Interestingly, chemogenetic activation of ABNs in Ascl1-hM3Dq mice significantly increased the time spent in the center of the open field (Fig. 6b) without alteration of locomotion (Fig. 6c), as compared with control mice. Moreover, activation of ABNs significantly increased time spent in the open arms of the zero maze (Fig. 6d) but failed to alter immobility time during the forced swimming test (Fig. 6e). These results suggest that ABN activity is sufficient for regulation of anxiety-like (but not depressive-like) behavior. In contrast, chemogenetic inhibition of ABNs in Ascl1-hM4Di mice significantly decreased the time spent in the center of the open field (Fig. 6f), without alteration of locomotion (Fig. 6g). In addition, such manipulation significantly decreased the time spent in the open arms of the zero maze (Fig. 6h) but failed to alter immobility time during the forced swimming test (Fig. 6i). These results suggest that ABN activity is required for anxiety-like (but not depressive-like) behaviors.

Next, similar sets of tests were performed to address whether activity of SuM-modified ABNs is involved in emotion processing, using the activity manipulation system mentioned above (Fig. 6j). Chemogenetic activation of SuM-modified ABNs in ChR2-Ascl1-hM3Dq mice significantly increased time spent in the center of the open field (Fig. 6k), as well as time spent in the open arms of the zero maze (Fig. 6m). In contrast, chemogenetic inhibition of ABNs in ChR2 mice decreased those times (Fig. 6o,q). Activation or inhibition of ABNs did not alter locomotion of ChR2 and control mice in the open field test (Fig. 6l,p). These results suggest that activity of SuM-modified ABNs is both sufficient and necessary for further modulation of anxiety-like behavior. We also performed a forced swimming test and found that activation or inhibition of ABNs did not alter immobility time (Fig. 6n,r), suggesting that activity of ABNs is neither sufficient nor necessary for further modulation of depressive-like behavior.

DG-projecting SuM neurons exhibit increased activity and firing frequency in a novel environment. Increased firing of SuM neurons was recently shown in response to contextual and social novelty[26]. Therefore, we wondered whether environmental novelty could modulate the activity of DG-projecting SuM neurons. We chose an enriched environment (EE) in this study, because EE not only carries environmental novelty but is also a well-established proneurogenic stimulus that exerts robust effects on hippocampal neurogenesis[11]. To label DG-projecting SuM neurons, we injected retroAAV-Cre into the DG and AAV-DIO-GFP into the SuM (Fig. 7a). Interestingly, EE significantly increased c-Fos expression in DG-projecting SuM neurons as compared with mice housed in the home cage (HC) (Fig. 7b,c). We then recorded calcium dynamics in DG-projecting SuM neurons by fiber photometry. Specifically, we injected retroAAV-Cre into the DG and AAV-DIO-GCaMP7f into the SuM to label DG-projecting SuM neurons (Fig. 7d). Consistent with c-Fos data, calcium activity in DG-projecting

Fig. 6 | Bidirectional manipulation of SuM circuit-modified ABNs further modulates anxiety-like behavior. a, Experimental protocol for chemogenetic activation or inhibition of ABNs at 32 dpi during behavioral tests in Ascl1-hM3Dq and Ascl1-hM4Di mice. **b**–**e**, Chemogenetic activation of ABNs reduced anxiety-like behavior but not depressive-like behavior. Shown are quantifications in tests, including time spent in the center area (**b**) and total locomotion (**c**) in the open field test, time spent in open arms in the zero maze test (**d**) and immobility time in the forced swimming test (**e**). $n = 14$ mice in hM3 group, $n = 11$ mice in Ascl1-hM3 group, two-sided unpaired *t*-test; **b**, $P = 0.0098$; **c**, $P = 0.8005$; **d**, $P = 0.0385$; **e**, $P = 0.6520$. **f**–**i**, Chemogenetic inhibition of ABNs promotes anxiety-like behavior but not depressive-like behavior. Shown are quantifications (**f**–**i** correspond to **b**–**e**). $n = 8$ mice in hM4 group, $n = 9$ mice in Ascl1-hM4 group, two-sided unpaired *t*-test; **f**, $P = 0.0400$; **g**, $P = 0.0608$; **h**, $P = 0.0375$; **i**, $P = 0.6160$. **j**, Experimental design for behavioral testing with chemogenetic activation or inhibition of ABNs following optogenetic stimulation of SuM neurons for 32 days in Ascl1-hM3Dq and Ascl1-hM4Di mice. **k**–**n**, Chemogenetic activation of circuit-modified ABNs by SuM stimulation further reduced anxiety-like behaviors. In the open field test, time spent in center area was increased after activation of SuM circuit-modified newborn neurons (**k**) in ChR2 mice, with no change in total locomotion (**l**). Activation of SuM circuit-modified ABNs in ChR2 mice increased time spent in open arms in the zero maze test (**m**) but did not change immobility time in the forced swimming test (**n**). $n = 8$ mice for each group, two-sided unpaired *t*-test; **k**, $P = 0.0144$; **l**, $P = 0.7478$; **m**, $P = 0.0249$; **n**, $P = 0.3287$. **o**–**r**, Chemogenetic inhibition of circuit-modified ABNs by SuM stimulation further regulated anxiety-like behaviors. Shown are the quantifications (**o**–**r** correspond to **k**–**n**). $n = 8$ mice for each group, two-sided unpaired *t*-test; **o**, $P = 0.0424$; **p**, $P = 0.8075$; **q**, $P = 0.0421$; **r**, $P = 0.9910$.

SuM neurons was significantly increased in EE mice as compared with HC-housed controls (Fig. 7e–g). These results suggest that DG-projecting SuM neurons are highly responsive to environmental novelty with increased activity.

To further address whether the firing rate of individual DG-projecting SuM neurons is increased in EE, in vivo multichannel spike recording was performed (Fig. 7h). DG-projecting SuM neurons were labeled with ChR2 by injection of retroAAV-Cre-GFP into the DG and AAV-DIO-ChR2-mCherry into the SuM. Single-unit activity was recorded in the SuM during low-frequency laser stimulation to induce antidromic spikes in mice with ChR2 expression in SuM (Fig. 7i). Interestingly, the majority of DG-projecting SuM neurons increased the firing rate in EE, from an averaged frequency of 6.2 Hz in HC to 9.2 Hz in EE (Fig. 7j–l).

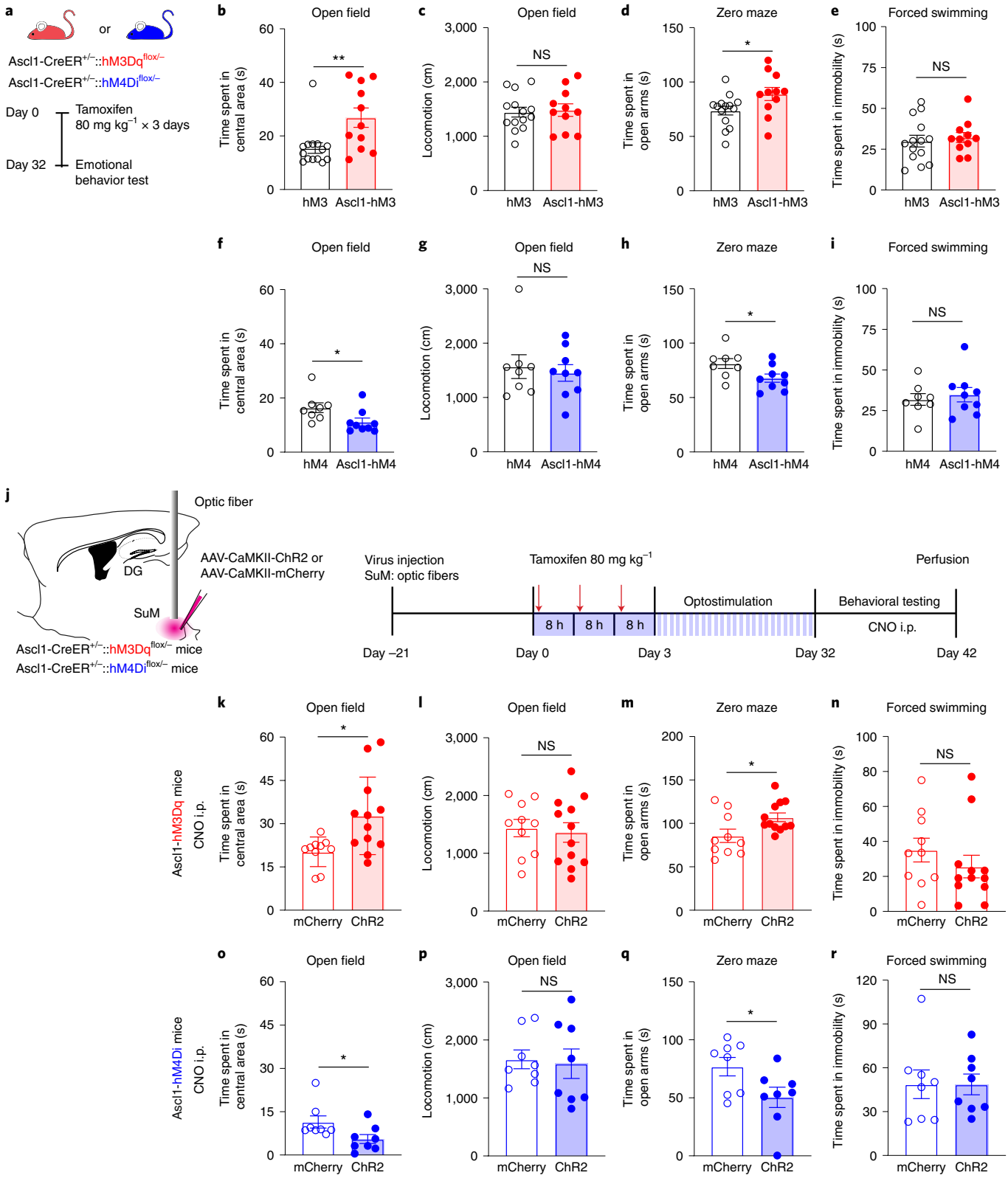

These results also serve as support for stimulation of SuM neurons at 10 Hz to mimic their firing rate in EE.

SuM is required for both baseline and environmental novelty-induced neurogenesis. Since SuM neurons are highly responsive to environmental novelty, we sought to address whether these are required for environmental novelty-induced effects on neurogenesis. Toward this direction, SuM neurons were ablated by injection of AAVs expressing CaMKII-caspase-3 and CaMKII-mCherry into the SuM of Ascl1-hM3Dq mice (Fig. 8a,b). Control Ascl1-hM3Dq mice were injected with AAV-CaMKII-mCherry. We first examined the density and maturation state of ABNs at 32 dpi in SuM-ablated and control mice housed in HC. SuM-ablated mice exhibited significantly reduced densities of HA^+ ABNs (Fig. 8c) and HA^+NeuN^+ ABNs (Fig. 8d) as compared with controls with intact SuM. These results suggest that the SuM is required for the production and maturation of ABNs under the baseline condition.

Consistent with the proneurogenic role of EE, increased densities of HA^+, HA^+NeuN^+ and HA^+DCX^+ cells were found in EE-exposed mice as compared with HC-housed controls (Fig. 8c–f), suggesting that EE promoted the production and maturation of ABNs. However, these EE-induced effects were abolished in SuM-ablated mice (Fig. 8c–f). These results suggest that EE-induced production and maturation of ABNs require intact SuM inputs.

SuM is required for ABN activity-dependent behavioral modulation under EE. Next, we examined ABN-mediated memory and anxiety-like behavior in mice housed in HC or exposed to EE and with intact or ablated SuM. Chemogenetic activation of ABNs in EE-housed mice with intact SuM increased discrimination ratio in the NPR test (Fig. 8g), freezing time in context A (but not in context B) at 24 h and 7 days in the CFC test (Fig. 8h–j), time spent in the center in the open field test (Fig. 8k) and time spent in the open arm in the zero maze (Fig. 8l), as compared with HC controls with intact SuM. By contrast, these ABN-mediated behavioral effects were abolished in SuM-ablated mice exposed to EE (Fig. 8g–l). Locomotion was also examined, but no significant changes were observed when comparing mice with intact and ablated SuM housed in HC (Fig. 8m), suggesting that ablation of the lateral SuM did not significantly affect locomotion under the baseline condition. Interestingly, EE significantly increased locomotion in SuM-ablated mice (Fig. 8m), suggesting that EE exerts SuM-independent effects on locomotion. Importantly, such SuM-independent effects on locomotion did not significantly alter memory and anxiety behaviors in SuM-ablated mice exposed to EE as compared with those housed in HC. Taken together, these results suggest that SuM neurons are required for spatial and contextual memory improvements and anxiolytic effects mediated by ABNs in EE-exposed mice.

Discussion

Adult hippocampal neurogenesis plays a critical role in memory and emotion processing and is dynamically regulated by neural circuit activity. Our study addresses a long-standing gap in the understanding of whether stimulation of neural circuits can generate sufficient neurogenic effects to modulate hippocampus-dependent behaviors. We identified a hypothalamic circuit that uses glutamate or GABA to enhance multiple stages of AHN (Extended Data Fig. 8), leading to increased production and enhanced maturation of ABNs. Importantly, in comparison with control ABN activity-dependent behavioral modulation, activation of SuM-promoted ABNs further enhanced memory performance and reduced anxiety-like behavior while inhibition of these ABNs exacerbated anxiety-like behavior without affecting memory performance. Furthermore, SuM neurons increased their activity and firing frequency in response to environmental novelty, and are required for EE-induced enhancement of neurogenesis. In addition, SuM neurons are required for ABN activity-dependent behavioral modulation under EE. Therefore, this key hypothalamic circuit is able to couple novelty signals to the production and maturation of ABNs and confers activity-dependent regulation of memory and emotional behaviors.

SuM neurons corelease GABA/glutamate onto mature GCs[25]. Interestingly, our slice recordings showed that adult-born cells receive SuM glutamate (rNSCs) or SuM GABA inputs (immature neurons), but not both. This is possibly due to a lack of either GABA receptors in the bushy processes of rNSCs or glutamate receptors in the dendritic compartments of immature neurons in the supragranular DG layer. High-resolution electron microscopy would be required to address these possibilities. Based on electrophysiological results, we speculate that SuM glutamate inputs promote rNSCs proliferation (symmetric and asymmetric) while SuM GABA inputs promote integration and maturation of early/mid-stage immature neurons. Because dual SuM glutamate/GABA or sole SuM glutamate inputs appear in ABNs only after 28 days, SuM glutamate probably does not play a major role in regulating the integration and maturation of ABNs. We speculate that SuM glutamate inputs are more important in regard to mature GCs, as our recent study showed that knockdown of SuM glutamate reduces GC activity[25]. Because some SuM neurons are capable of releasing substance P (SP)[31,51], it is possible that SuM neurons may release SP following patterned optostimulation, thus impacting AHN[52]. Future SP knockdown studies in SuM neurons could address SuM SP regulation of AHN.

Our study, using the chemogenetic approach, showed that activation of ABNs improves memory performance. However, a recent study using an optogenetic approach to activate ABNs found impaired memory performance[7]. This discrepancy could be explained by the differences in activity patterns of ABNs induced by chemogenetic versus optogenetic approaches. Furthermore, we used Ascl1CreER to target neurogenic rNSC population and early progenitors while Danielson et al.[7] used Nestin-CreER to predominantly target quiescent rNSCs. ABNs derived from the Nestin lineage may exhibit more maturational heterogeneity than those derived from Ascl1. Subsequently, optogenetic stimulation of heterogeneous ABNs may disrupt synchronized firing patterns, leading

Fig. 7 | DG-projecting SuM neurons exhibit increased activity in EE. a, Diagram of c-Fos labeling in DG-projecting SuM neurons in the EE. RetroAAV2-Cre and AAV5-DIO-eGFP were injected into the DG and SuM, respectively. Mice were held in EE for 15 min and perfused 75 min later for c-Fos staining. Control mice were held in HC. Scale bar, 100 µm. **b**, Representative images of c-Fos expression in the SuM in EE and HC. Yellow arrowheads indicate $c\text{-}Fos^+GFP^+$ cells. Scale bar, 20 µm. **c**, Expression of c-Fos in DG-projecting SuM neurons was significantly increased in EE. $n = 4$ mice per group, $P = 0.0002$ by two-sided unpaired *t*-test. **d**, Diagram of calcium recording of DG-projecting SuM neurons. RetroAAV2-Cre and AAV5-DIO-GCaMP7f were injected into the DG and SuM, respectively. Fiber photometry recording of free-moving mice in HC and EE for 10 min. Scale bar, 100 µm. **e**, Representative traces of population activity of DG-projecting SuM neurons in the HC and EE. **f**,**g**, Average peak $\Delta F/F$ (**f**) and events (**g**) of calcium activity in HC and EE. $n = 8$ mice per group, two-sided paired *t*-test, $P = 0.0772$ (**f**), $P = 0.0081$(**g**). **h**, Diagram of in vivo multichannel spike recording. AAV2-retro-Cre-GFP and AAV5-DIO-ChR2-mCherry were injected into the DG and SuM, respectively. Optic fibers and tetrodes were implanted above or into the SuM, respectively. Sample image showing SuM with optical tetrode locations. **i**, Peristimulus time histograms of representative single units photoidentified as SuM-DG projectors. **j**, Waveforms of spontaneous (black line denotes mean, gray shaded area s.d.) and light-evoked (blue) spikes of single units. **k**, Raster plots of sample neurons. **l**, Firing rate (FR) of DG-projecting SuM neurons in HC and EE. $n = 12$ neurons from six mice. $P = 0.0234$ by two-sided paired *t*-test.

to aberrant information processing within the hippocampal circuits and impaired memory performance.

We showed that increased activity of SuM-promoted ABNs further modulates major hippocampal functions, such as memory and emotion processing. Interestingly, without activity manipulation, SuM-modified ABNs failed to alter memory and anxiety-like behavior (Extended Data Fig. 9a–j). By contrast, chronic SuM inhibition impairs the production and maturation of ABNs, which correlates

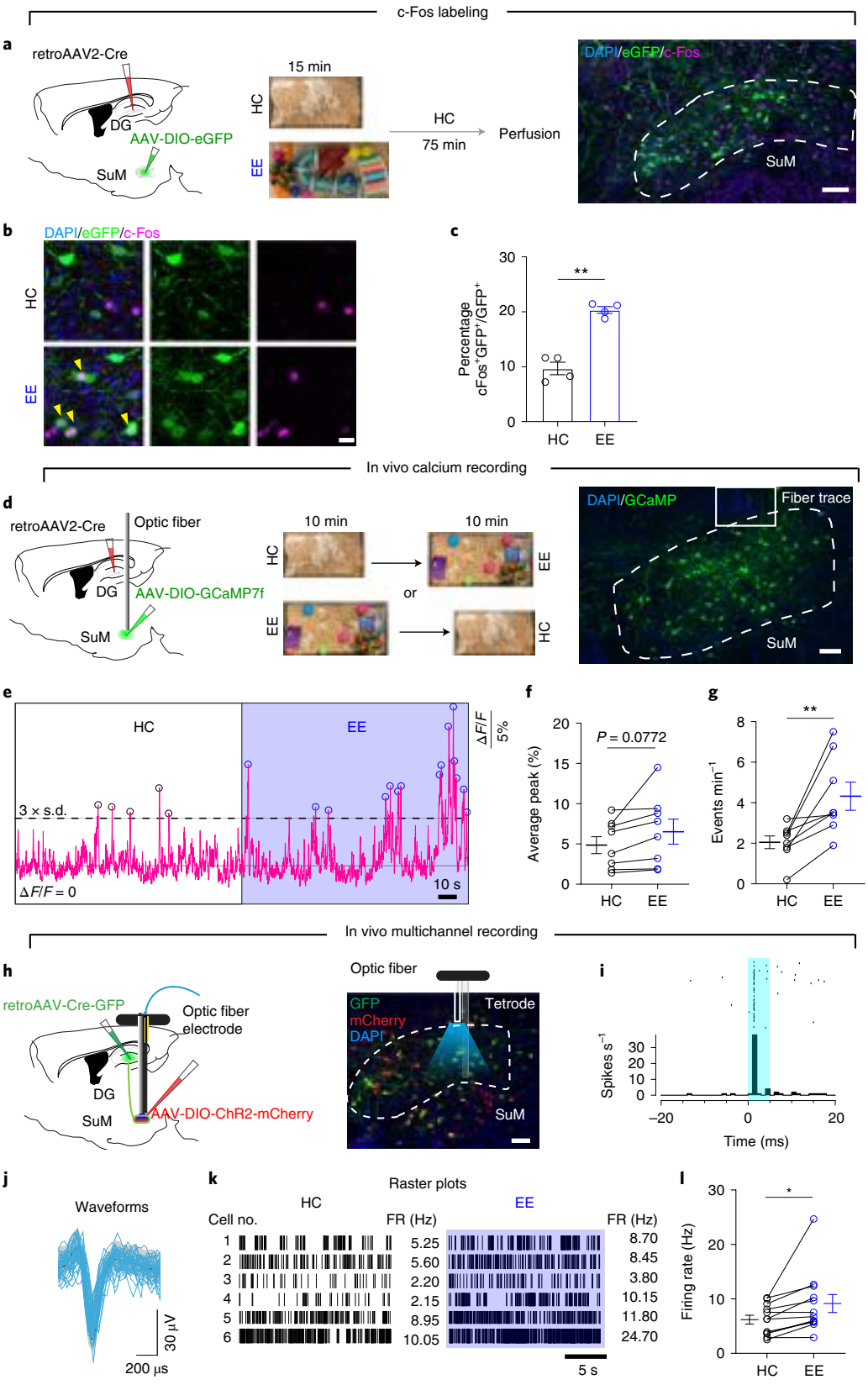

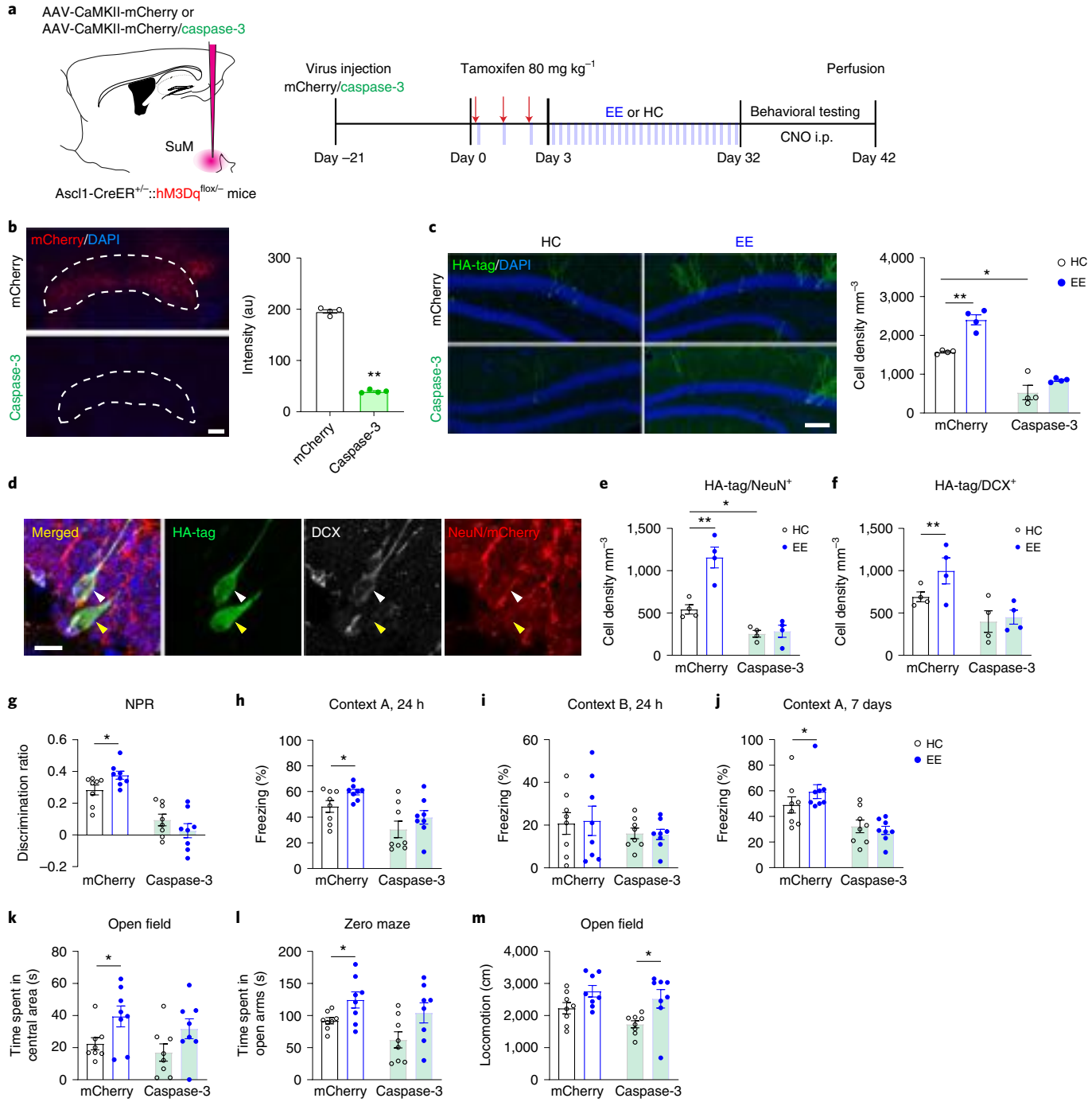

Fig. 8 | Ablation of SuM neurons abolishes EE-induced neurogenic effects and behavioral improvement mediated by ABNs. a, Experimental design for behavioral testing following chemogenetic activation of ABNs after ablation of SuM neurons in Ascl1-hM3Dq mice. **b**, Fluorescence of mCherry in the SuM with/without caspase-3 expression. Scale bar, 100 μm. $n = 4$ mice per group, $P < 0.0001$ by two-sided unpaired t-test. **c**, Sample images and density quantification of HA-tag$^+$ Ascl1-hM3Dq cells in the DG of mCherry-control and SuM-ablated (caspase-3) mice in HC or EE. Scale bar, 100 μm. $n = 4$ mice per group; $^*P < 0.05$, $^{**}P < 0.01$ by two-way ANOVA followed by Tukey's post hoc test. **d**, Sample images of HA-tag/DCX/NeuN staining in the DG. The white arrowhead indicated an HA-tag$^+$DCX$^+$ cell; the yellow arrowhead indicated an HA-tag$^+$DCX$^+$NeuN$^+$ cell. Scale bar, 10 μm. **e**,**f**, Density quantification of HA-tag/NeuN$^+$ (**e**) and HA-tag/DCX$^+$ cells(**f**) in Ascl1-hM3Dq mice. $n = 4$ mice per group; $^*P < 0.05$, $^{**}P < 0.01$ by two-way ANOVA, followed by Tukey's post hoc test. **g**, Discrimination of NPR tests after chemogenetic activation of ABNs in Ascl1-hM3Dq HC/EE mice following SuM mCherry/caspase-3 expression. $n = 8$ mice per group; $^*P < 0.05$, $^{**}P < 0.01$ by two-way ANOVA followed by Tukey's post hoc test. **h**–**j**, Freezing time in context A (**h**) and context B (**i**) at 24 h, and in context A at 7 days (**j**) after chemogenetic activation of ABNs in Ascl1-hM3Dq HC/EE mice following SuM mCherry/caspase-3 expression. $n = 8$ mice per group; $^*P < 0.05$, $^{**}P < 0.01$ by two-way ANOVA followed by Tukey's post hoc test. **k**–**m**, Quantifications of time spent in center area in open field test (**k**), time spent in open arms in zero maze test (**l**) and total locomotion (**m**) in open field test following chemogenetic activation of ABNs in Ascl1-hM3Dq HC/EE mice upon SuM mCherry/caspase-3 expression. $n = 8$ mice per group; $^*P < 0.05$, $^{**}P < 0.01$ by two-way ANOVA followed by Tukey's post hoc test.

with impaired spatial memory and increased anxiety (Extended Data Fig. 10). Together, these results suggest that spatial memory and anxiety states are more sensitive to SuM loss-of-function ABNs (reduced number and maturity) than SuM gain-of-function ABNs (increased number and maturity). Supporting this notion, previous studies in mice with increased numbers of ABNs also reported no alteration in major memory tasks (that is, NPR and CFC). Differences were observed only in subtle memory tasks designed to test pattern separation from similar contexts[53]. Therefore, it is possible that our behavioral assays may not have sufficient resolution to detect subtle memory improvements from SuM gain-of-function ABNs without ABN activity modulation. These results highlight that the activity of ABNs is required for them to become engaged in behavior. This raises a crucial question as to whether the activity of ABNs can be elevated physiologically in vivo. Along with previous studies showing that running can increase ABN activity[7,54], we also found that c-Fos expression was increased in DCX^+ ABNs of EE-housed mice as compared with HC-housed mice (Extended Data Fig. 9k,l).

Interestingly, while ABN activity is both sufficient and necessary for regulation of spatial memory retrieval, it is sufficient (but not necessary) only for contextual memory, suggesting that it may play differential roles in regulation of spatial versus contextual memory. Supporting this notion, a recent study showed that in response to lateral entorhinal cortex (LEC)-mediated contextual inputs, ABNs inhibited mature GCs, while in response to medial entorhinal cortex (MEC)-mediated spatial inputs, ABNs excited mature GCs[55]. Therefore, it is possible that inhibition of ABNs may abolish the excitation of mature GCs in response to MEC-mediated spatial inputs. By contrast, such manipulation may not be able to further inhibit mature GCs in response to LEC-mediated contextual inputs due to the potential floor effect, because mature GCs generally have low activity. Whether increased structural maturation of neurocircuit-modified ABNs alters the likelihood of them becoming activated by distinct entorhinal afferents remains to be determined.

In conclusion, our study identifies a key subcortical region in the hypothalamus that can be manipulated to enhance adult hippocampal neurogenesis. It also highlights the important role of ABN activity in the modulation of memory and emotional states.

Online content

Any methods, additional references, Nature Research reporting summaries, source data, extended data, supplementary information, acknowledgements, peer review information; details of author contributions and competing interests; and statements of data and code availability are available at https://doi.org/10.1038/s41593-022-01065-x.

Received: 23 March 2021; Accepted: 29 March 2022;
Published online: 6 May 2022

References

1. Ming, G. L. & Song, H. Adult neurogenesis in the mammalian brain: significant answers and significant questions. *Neuron* **70**, 687–702 (2011).
2. van Praag, H. et al. Functional neurogenesis in the adult hippocampus. *Nature* **415**, 1030–1034 (2002).
3. Drew, L. J., Fusi, S. & Hen, R. Adult neurogenesis in the mammalian hippocampus: why the dentate gyrus? *Learn. Mem.* **20**, 710–729 (2013).
4. Schmidt-Hieber, C., Jonas, P. & Bischofberger, J. Enhanced synaptic plasticity in newly generated granule cells of the adult hippocampus. *Nature* **429**, 184–187 (2004).
5. Ge, S., Yang, C. H., Hsu, K. S., Ming, G. L. & Song, H. A critical period for enhanced synaptic plasticity in newly generated neurons of the adult brain. *Neuron* **54**, 559–566 (2007).
6. Marin-Burgin, A., Mongiat, L. A., Pardi, M. B. & Schinder, A. F. Unique processing during a period of high excitation/inhibition balance in adult-born neurons. *Science* **335**, 1238–1242 (2012).
7. Danielson, N. B. et al. Distinct contribution of adult-born hippocampal granule cells to context encoding. *Neuron* **90**, 101–112 (2016).
8. Gu, Y. et al. Optical controlling reveals time-dependent roles for adult-born dentate granule cells. *Nat. Neurosci.* **15**, 1700–1706 (2012).
9. Temprana, S. G. et al. Delayed coupling to feedback inhibition during a critical period for the integration of adult-born granule cells. *Neuron* **85**, 116–130 (2015).
10. van Praag, H., Kempermann, G. & Gage, F. H. Running increases cell proliferation and neurogenesis in the adult mouse dentate gyrus. *Nat. Neurosci.* **2**, 266–270 (1999).
11. Kempermann, G., Kuhn, H. G. & Gage, F. H. More hippocampal neurons in adult mice living in an enriched environment. *Nature* **386**, 493–495 (1997).
12. Santarelli, L. et al. Requirement of hippocampal neurogenesis for the behavioral effects of antidepressants. *Science* **301**, 805–809 (2003).
13. Christian, K. M., Song, H. & Ming, G. L. Functions and dysfunctions of adult hippocampal neurogenesis. *Annu. Rev. Neurosci.* **37**, 243–262 (2014).
14. Song, J., Christian, K. M., Ming, G. L. & Song, H. Modification of hippocampal circuitry by adult neurogenesis. *Dev. Neurobiol.* **72**, 1032–1043 (2012).
15. Bao, H. & Song, J. Treating brain disorders by targeting adult neural stem cells. *Trends Mol. Med.* **24**, 991–1006 (2018).
16. Song, J., Olsen, R. H., Sun, J., Ming, G. L. & Song, H. Neuronal circuitry mechanisms regulating adult mammalian neurogenesis. *Cold Spring Harb. Perspect. Biol.* https://doi.org/10.1101/cshperspect.a018937 (2016).
17. Davis, K. D. et al. Globus pallidus stimulation activates the cortical motor system during alleviation of parkinsonian symptoms. *Nat. Med.* **3**, 671–674 (1997).
18. Vidailhet, M. et al. Bilateral deep-brain stimulation of the globus pallidus in primary generalized dystonia. *N. Engl. J. Med.* **352**, 459–467 (2005).
19. Mayberg, H. S. et al. Deep brain stimulation for treatment-resistant depression. *Neuron* **45**, 651–660 (2005).
20. Song, J. et al. Neuronal circuitry mechanism regulating adult quiescent neural stem-cell fate decision. *Nature* **489**, 150–154 (2012).
21. Song, J. et al. Parvalbumin interneurons mediate neuronal circuitry-neurogenesis coupling in the adult hippocampus. *Nat. Neurosci.* **16**, 1728–1730 (2013).
22. Bao, H. et al. Long-range GABAergic inputs regulate neural stem cell quiescence and control adult hippocampal neurogenesis. *Cell Stem Cell* **21**, 604–617 (2017).
23. Asrican, B. et al. Neuropeptides modulate local astrocytes to regulate adult hippocampal neural stem cells. *Neuron* **108**, 349–366 (2020).
24. Yeh, C. Y. et al. Mossy cells control adult neural stem cell quiescence and maintenance through a dynamic balance between direct and indirect pathways. *Neuron* **99**, 493–510 (2018).
25. Zheng, J. et al. Interneuron accumulation of phosphorylated tau impairs adult hippocampal neurogenesis by suppressing GABAergic transmission. *Cell Stem Cell* **26**, 331–345 (2020).
26. Chen, S. et al. A hypothalamic novelty signal modulates hippocampal memory. *Nature* **586**, 270–274 (2020).
27. Root, D. H. et al. Selective brain distribution and distinctive synaptic architecture of dual glutamatergic-GABAergic neurons. *Cell Rep.* **23**, 3465–3479 (2018).
28. Ito, H. T., Moser, E. I. & Moser, M. B. Supramammillary nucleus modulates spike-time coordination in the prefrontal-thalamo-hippocampal circuit during navigation. *Neuron* **99**, 576–587 (2018).
29. Hashimotodani, Y., Karube, F., Yanagawa, Y., Fujiyama, F. & Kano, M. Supramammillary nucleus afferents to the dentate gyrus co-release glutamate and gaba and potentiate granule cell output. *Cell Rep.* **25**, 2704–2715 (2018).
30. Pedersen, N. P. et al. Supramammillary glutamate neurons are a key node of the arousal system. *Nat. Commun.* **8**, 1405 (2017).
31. Farrell, J. S. et al. Supramammillary regulation of locomotion and hippocampal activity. *Science* **374**, 1492–1496 (2021).
32. Li, Y. et al. Supramammillary nucleus synchronizes with dentate gyrus to regulate spatial memory retrieval through glutamate release. *eLife* https://doi.org/10.7554/eLife.53129 (2020).
33. Encinas, J. M. & Enikolopov, G. Identifying and quantitating neural stem and progenitor cells in the adult brain. *Methods Cell. Biol.* **85**, 243–272 (2008).
34. Soussi, R., Zhang, N., Tahtakran, S., Houser, C. R. & Esclapez, M. Heterogeneity of the supramammillary-hippocampal pathways: evidence for a unique GABAergic neurotransmitter phenotype and regional differences. *Eur. J. Neurosci.* **32**, 771–785 (2010).
35. Vertes, R. P. Major diencephalic inputs to the hippocampus: supramammillary nucleus and nucleus reuniens. Circuitry and function. *Prog. Brain Res.* **219**, 121–144 (2015).
36. Kim, E. J., Leung, C. T., Reed, R. R. & Johnson, J. E. In vivo analysis of Ascl1 defined progenitors reveals distinct developmental dynamics during adult neurogenesis and gliogenesis. *J. Neurosci.* **27**, 12764–12774 (2007).
37. Shin, J. et al. Single-cell RNA-seq with waterfall reveals molecular cascades underlying adult neurogenesis. *Cell Stem Cell* **17**, 360–372 (2015).

38. Bond, A. M., Ming, G. L. & Song, H. Adult mammalian neural stem cells and neurogenesis: five decades later. *Cell Stem Cell* **17**, 385–395 (2015).
39. Kim, E. J., Ables, J. L., Dickel, L. K., Eisch, A. J. & Johnson, J. E. Ascl1 (Mash1) defines cells with long-term neurogenic potential in subgranular and subventricular zones in adult mouse brain. *PLoS ONE* **6**, e18472 (2011).
40. Pilz, G. A. et al. Live imaging of neurogenesis in the adult mouse hippocampus. *Science* **359**, 658–662 (2018).
41. Bottes, S. et al. Long-term self-renewing stem cells in the adult mouse hippocampus identified by intravital imaging. *Nat. Neurosci.* **24**, 225–233 (2021).
42. Ge, S. et al. GABA regulates synaptic integration of newly generated neurons in the adult brain. *Nature* **439**, 589–593 (2006).
43. Kim, J. Y. et al. Interplay between DISC1 and GABA signaling regulates neurogenesis in mice and risk for schizophrenia. *Cell* **148**, 1051–1064 (2012).
44. Kumar, D. et al. Sparse activity of hippocampal adult-born neurons during REM sleep is necessary for memory consolidation. *Neuron* **107**, 552–565 (2020).
45. Lods, M. et al. Adult-born neurons immature during learning are necessary for remote memory reconsolidation in rats. *Nat. Commun.* **12**, 1778 (2021).
46. Anacker, C. & Hen, R. Adult hippocampal neurogenesis and cognitive flexibility – linking memory and mood. *Nat. Rev. Neurosci.* **18**, 335–346 (2017).
47. Wang, G., Wang, C., Chen, H., Chen, L. & Li, J. Activation of 6-8-week-old new mature adult-born dentate granule cells contributes to anxiety-like behavior. *Neurobiol. Stress* **15**, 100358 (2021).
48. Tunc-Ozcan, E. et al. Activating newborn neurons suppresses depression and anxiety-like behaviors. *Nat. Commun.* **10**, 3768 (2019).
49. Armbruster, B. N., Li, X., Pausch, M. H., Herlitze, S. & Roth, B. L. Evolving the lock to fit the key to create a family of G protein-coupled receptors potently activated by an inert ligand. *Proc. Natl Acad. Sci. USA* **104**, 5163–5168 (2007).
50. Zhu, H. et al. Cre-dependent DREADD (Designer Receptors Exclusively Activated by Designer Drugs) mice. *Genesis* **54**, 439–446 (2016).
51. Borhegyi, Z. & Leranth, C. Distinct substance P- and calretinin-containing projections from the supramammillary area to the hippocampus in rats; a species difference between rats and monkeys. *Exp. Brain Res.* **115**, 369–374 (1997).
52. Park, S. W., Yan, Y. P., Satriotomo, I., Vemuganti, R. & Dempsey, R. J. Substance P is a promoter of adult neural progenitor cell proliferation under normal and ischemic conditions. *J. Neurosurg.* **107**, 593–599 (2007).
53. Sahay, A. et al. Increasing adult hippocampal neurogenesis is sufficient to improve pattern separation. *Nature* **472**, 466–470 (2011).
54. Shevtsova, O., Tan, Y. F., Merkley, C. M., Winocur, G. & Wojtowicz, J. M. Early-age running enhances activity of adult-born dentate granule neurons following learning in rats. *eNeuro* https://doi.org/10.1523/Eneuro.0237-17.2017 (2017)
55. Luna, V. M. et al. Adult-born hippocampal neurons bidirectionally modulate entorhinal inputs into the dentate gyrus. *Science* **364**, 578–583 (2019).

Methods

Animals. Single- or double-transgenic mice (6–14 weeks, males and females) were used for all experiments from the following genetically modified mouse lines: Vgat-Cre (B6, Slc32a1tm2(cre)Lowl/J), Ascl1CreER[36,39] (B6) and Ai9 (B6), obtained from the Jackson laboratory; hM4Di-flox[50] (R26-LSL-Gi-DREADD, B6) and hM3Dq-flox[50] (R26-LSL-Gq-DREADD, B6) mice were obtained from Bryan Roth's laboratory at the University of North Carolina at Chapel Hill; and Nestin-GFP[32] (B6) mice were obtained from G. Enikolopov at Stony Brook University. Ascl1CreER mice were mated to Ai9, hM3Dq-flox or hM4Di-flox mice to get Ascl1CreER::Ai9, Ascl1CreER::hM3Dq-flox (Ascl1-hM3Dq) or Ascl1CreER::hM4Di-flox (Ascl1-hM4Di) mice. Only Ascl1CreER heterozygous mice were used in experiments. No immune deficiencies or other health problems were observed in these lines, and all animals were experimentally and drug naive before use. Animals were group housed and bred in a dedicated husbandry facility under 12/12-h light/dark cycles with food and water ad libitum and under veterinary supervision. Behavior tests were performed in the light phase. Animals subjected to surgical procedures were moved to a satellite housing facility for recovery under the same light/dark cycle. All procedures were conducted in accordance with the NIH Guide for the Care and Use of Laboratory Animals and with the approval of the Institutional Animal Care and Use Committee at the University of North Carolina at Chapel Hill.

Stereotaxic surgery. Mice were anesthetized under 1.5–2.0% isoflurane in oxygen at a flow rate of 0.8 l min^{-1}. Virus was injected by microsyringe (Hamilton, 33GA) and microinjection pump (Harvard Apparatus) at a rate of 30–50 nl min^{-1} with the following coordinates: virus was injected unilaterally/bilaterally into the lateral SuM (anteroposterior (AP), −2.4 mm; mediolateral (ML), ±0.6 mm; dorsoventral (DV), −4.85 mm) or DG (AP, −2.0 mm; ML, ±1.4 mm; DV, −2.0 mm). A total viral volume of 150–250 nl was delivered to each site, with the needle left in the site for at least 10 min to permit diffusion. All coordinates were based on values from The Mouse Brain Stereotaxic Coordinates.

For in vivo fiber photometry recording, retroAAV2-Cre (Addgene) was injected into the DG and AAV5-DIO-GCaMP7 into the SuM. Unilateral optic fibers (Newdoon Inc.; ferrule outside diameter (OD), 1.25 mm; core, 200 µm; numerical aperture (NA), 0.37) were implanted in the SuM (AP, −2.4 mm; ML, +0.6 mm; DV, −4.85 mm).

For in vivo multichannel recording by optic tetrodes, AAV2-retro-Cre-GFP was injected into the DG and AAV5-DIO-ChR2-mCherry into the SuM.

For in vivo optogenetics, either bilateral optic fibers (Newdoon Inc.; OD, 1.25 mm; core, 200 µm; NA, 0.37) were implanted above the DG (AP −2.0 mm, ML ±1.4 mm, DV −1.7 mm) or unilateral optic fibers were implanted above the SuM (AP, −2.4 mm; ML, +0.6 mm; DV, −4.5 mm). We unilaterally stimulated SuM neurons only, because these send almost equal projections to the bilateral DG. After 3 weeks of recovery, mice were used for in vivo optogenetic stimulation.

For analysis of caspase lesions, mixed CaMKII-caspase-3 (AAV5-CaMKII-Cre/FLEX-caspase-3/DIO-mCherry) virus was bilaterally injected into the SuM. For mCherry control, AAV5-CaMKII-mCherry was injected into the SuM.

Fiber photometry recording and analysis. After 3 weeks of injecting retroAAV2-Cre into the DG and AAV5-DIO-GCaMP7f into the SuM, fiber photometry recording was carried out using a commercial device (RWD life science) as previously described[25,56,57]. In brief, 470- and 410-nm laser beams were first launched into the fluorescence cube then into the optical fibers; the 410-nm laser was used for motion control. GCaMP and control emission fluorescence was collected by the camera at 20 Hz. In vivo recordings were carried out in an open-top HC (21.6 × 17.8 × 12.7 cm^3) or EE (45 × 25 × 20 cm^3) containing toys, colorful balls, domes or tunnels and food, for 10 min. We derived the value of the photometry signal F as F_{470}/F_{410}, calculating $\Delta F/F = (F - F_0)/F_0$, where F_0 is the median of the photometry signal. Only calcium signals >3 s.d. was treated as events. The average of ten peak $\Delta F/F$ values and the number of events per minute for each mouse were analyzed.

In vivo multichannel recording by optic tetrodes. To record the activity of DG-projecting SuM neurons, we used a custom-built optrode consisting of an optical fiber (0.2-mm diameter) surrounded by 16 microwire electrodes (13 µm; Sandivik, no. PX000003) twisted into tetrodes. The tetrode wire tips were plated with gold to adjust impedance to 500–800 kΩ. Note that wire tips were 0.5 mm longer than the optical fiber end, to achieve efficient photostimulation of recorded neurons in vivo.

For implantation the electrode was slowly advanced into the SuM under the control of a piezoelectric micromanipulator (Scientifica). The optical fiber and electrodes were inserted into a screw-driven microdrive. The optrode was slowly lowered in 30 ± 10 µm steps to search for light-responsive neurons. Multichannel signals were digitalized at 40 kHz and recorded simultaneously on a 16-channel Plexon system and Omniplex software (CED, Plexon) with polysomnographic recordings (digitized at 1 kHz).

Spikes were sorted offline on the basis of waveform energy and the first three principal components of a spike waveform on each tetrode channel. Single units were identified using the built-in principal component analysis in Offline Sorter software (Plexon). The quality of each unit was assessed by the presence of a refractory period, and quantified using isolation distance and L-ratio. Units with an isolation distance <20 or L-ratio >0.1 were discarded.

To identify ChR2-tagged neurons, laser pulse trains (10 Hz, with a duration of 5 ms) were delivered every 1 min. A unit was identified as a ChR2-tagged neuron when spikes were evoked by laser pulses at short first-spike latency (<6 ms), if the waveforms of the laser-evoked and spontaneous spikes were highly similar.

Chemical administration and optogenetic/chemogenetic stimulation protocol. For optogenetic stimulation of SuM-DG projections, a 10-Hz, 5-ms duration, 473-nm blue light stimulation paradigm was given for 30 s ON/270 s OFF for 8 h d^{-1} for 3 days. On day 3, animals were given four doses of EdU (40 mg kg^{-1}) at 2-h intervals by intraperitoneal (i.p.) injection and perfused 2 h after the last injection of EdU. For chemogenetic activation and inhibition of SuM neurons, CNO (1 mg kg^{-1}) was administrated by i.p. injection for 5 days. On day 5, animals were given four doses of EdU (40 mg kg^{-1}) at 2-h intervals by i.p. injection and perfused 2 h after the last injection of EdU.

For lineage-tracing experiments, 473-nm blue light stimulation at 10 Hz, 5-ms pulses, 30 s per 5 min was given as below. For 3-day post-tamoxifen injection (dpi) and 42 dpi experiments, blue light stimulations were given for 8 h d^{-1} for 3 days with tamoxifen injection i.p. at 80 mg kg^{-1} (total of three injections). Mice were perfused on either day 3 or 42 after the first tamoxifen injection. For 16 dpi experiments, blue light was applied for 8 h d^{-1}for the first 3 days and 40 mg kg^{-1} tamoxifen was given by i.p. injection over the first 2 days. Here we used a lower dosage of tamoxifen because less dense newborn immature neurons were needed for further morphology analysis. From days 4–16, blue light stimulations were given for 2 h d^{-1} and mice were perfused on day 16 immediately after stimulation. For 32 dpi experiments, blue light was given for 8 h for the first 3 days with i.p. tamoxifen (80 mg kg^{-1}). From days 4–32, blue light stimulation was given for 2 h d^{-1} and mice were perfused on day 32 immediately after light stimulation. For EE, mice were placed with toys, colorful balls, domes, or tunnels with free access to running dishes for 8 h d^{-1} in the first 3 days and 2 h d^{-1} for the next 29 days. Novel objects were introduced to the cage every day to ensure the novelty.

For circuit-modified, wild-type mice and Ascl1-hM3Dq and Ascl1-hM4Di mice, blue light was applied for 8 h for the first 3 days with i.p. tamoxifen (80 mg kg^{-1}). From days 4–32, blue light stimulation was given for 2 h d^{-1}. Behavior tests were performed after day 32. For chemogenetic activation or inhibition of DG newborn neurons, CNO (0.5 mg or 1.0 mg kg^{-1}) was administered to Ascl1-hM3Dq or Ascl1-hM4Di mice by i.p. injection 30–60 min before behavior tests, respectively.

For chronic inhibition of SuM neurons, CNO was provided in the drinking water at a concentration of 5 mg 200 ml^{-1} for 32 days, with i.p. tamoxifen (80 mg kg^{-1}) for the first 3 days. Mice weighing ~25–30 g consumed about 4 ml of water per day and received 4 mg kg^{-1} d^{-1} CNO. Behavior tests were performed 1 day after CNO administration. Mice were perfused after behavior tests to examine virus expression and count ABNs.

For all experiments, brain sections were collected to check virus expression, perform mCitrine/HA-tag or for c-Fos staining.

Immunohistochemistry. Fixed brain samples were collected following perusion with 4% paraformaldehyde (PFA). Briefly, mice were exposed to a lethal dose of isoflurane in an incubation chamber. At cessation of breathing, the chest cavity was exposed, a 27G needle inserted into the left ventricle and PBS (~20 ml) first instilled by peristaltic pump, followed by freshly made 4% PFA (~20 ml, in PBS) via the same line. The brain was extracted and placed in 10 ml of 4% PFA for overnight incubation and then switched to 30% sucrose for 2–3 days, fully submerged. Brains were sectioned on a microtome at a thickness of 40 µm and then stored in antifreeze solution at −20 °C until further usage.

Sections designated for free-floating antibody staining were subjected to the following pretreatment steps: three 5-min incubations in 1 mg ml^{-1} sodium borohydride in PBS, then two >1-h incubations in 0.3% Triton-X in PBS. A blocking step was then performed using 5% donkey serum in 0.1% PBST. Sections were then transferred to the primary antibody solution in 0.1% PBST and kept at 4 °C for 48 h, with intermittent brief periods of shaking. After primary incubation, sections were subjected to three 30-min wash steps in 0.1% PBST. Sections were then transferred to a secondary antibody solution in 0.1% PBST for 2 h at 24 °C, with intermittent brief periods of shaking. Sections were washed three times for 30 min each in 0.1% PBT, with 1 µM DAPI solution included on the third wash step. Sections were mounted on charged glass slides using Diamond prolong gold mounting medium (Thermo Fisher Scientific, no. P36961) and no. 1.5 glass coverslips (Electron Microscopy Sciences, no. 72204-02).

For c-Fos labeling, mice were perfused for 90 min after CNO injection. For EE experiments, mice were held in EE for 15 min and perfused 75 min later. A rabbit c-Fos antibody (Synaptic System, no. 226003) was used at a dilution of 1:1,000.

For EdU labeling, slides were incubated in EdU click reaction buffer (0.1 M Tris, 0.5–1.0 mM $CuSO_4$, 10 µM 488 Alexa azide fluorescent-azide and 100 mM ascorbic acid) for 2 h. After washing, antibody staining steps were performed similarly to those described for floating sections.

For 3 dpi experiments, brain sections were processed by immunohistochemistry for Ki67 Rabbit (Anti-Rabbit Ki67, Thermo Fisher Scientific, 1:500), Sox2 Goat

(Anti-Goat Sox2, Santa Cruz Biotechnology, 1:1,000) and GFAP Mouse (Anti-Goat GFAP, Santa Cruz Biotechnology, 1:1,000). Sox2 and GFAP were both placed in the far-red channel using a mixture of Alexa 647 secondaries of both species; these can be distinguished because Sox2 is exclusively nuclear whereas GFAP is exclusively cytoplasmic. For 16 dpi experiments, DCX were stained with anti-Goat DCX (Santa Cruz Biotechnology, 1:500) in the 647 channel. For 32 dpi experiments, anti-Mouse NeuN (Millipore, no. MAB377, 1:500) in the 488 channel and anti-Goat DCX in the 647 channel were stained.

For HA-tag staining, a rabbit HA-tag antibody (Cell Signaling Technology, no. 3724) was used at 1:500 to label Ascl1-hM3Dq and Ascl1-hM4Di cells.

For biocytin staining, brain slices were fixed overnight with 4% paraformaldehyde in PBS after whole-cell patch-clamp recording. Slices were rinsed with PBS and then incubated with Alexa Fluor 647 streptavidin and DAPI for 6 h at room temperature. After rinsing, slices were dried on a slide glass and coverslipped. All brain slices were imaged with an Olympus FV3000 microscope.

Quantifications. All image analyses were performed blind to the experimental group. Confocal data sets were loaded into ImageJ (FIJI). Cells from the whole DG were counted from five sections, including three dorsal and two ventral. Cell density was normalized by the volume of DG (area of DAPI/slice × stacks). Cells were counted using the Cell Counter plugin in ImageJ. EdU, nestin, DCX, EdU$^+$nestin$^+$ and Edu$^+$DCX$^+$ cells were counted. For lineage analysis, cells were counted as below:

(1) For 3 dpi experiments, total numbers of tdTomato$^+$ and K167$^+$tdTomato$^+$ cells were counted per section. tdTomato$^+$ cells were defined as one of two types: (1) rNSCs were GFAP $^+$radial process cells, which denote radial glia-like cells (RGLs) (Ki67$^+$tdTomato$^+$GFAP$^+$ and tdTomato$^+$GFAP$^+$ cells were counted); and (2) type 2 progenitors were Sox2$^+$, nonradial cells, located in the SGZ or within 10–15 µm below the SGZ into the hilus, which are progenitors (Ki67$^+$tdTomato$^+$Sox2$^+$ nonradial cells and tdTomato$^+$Sox2$^+$ nonradial cells were counted).

(2) For 16 dpi experiments, total numbers of tdTomato$^+$ cells was counted per section then DCX$^+$tdTomato$^+$ and DCX$^-$tdTomato$^+$ cells were counted. Sholl analysis was performed for DCX$^+$tdTomato$^+$ cells.

(3) For 32 dpi experiments, total numbers of tdTomato$^+$ mature and immature neurons were counted per section then NeuN$^+$, DCX$^+$, NeuN$^+$DCX$^+$ and NeuN$^+$DCX$^-$tdTomato$^+$ cells were counted.

(4) For 42 dpi experiments, total numbers of tdTomato$^+$ neurons were counted per section.

(5) For Ascl1-hM3Dq mice, mCitrine (by staining with GFP)-labeled cells were counted; for Ascl1-hM4Di mice, HA-tag labeled cells were counted. In SuM ablation experiments, HA-tag, DCX$^+$HA-tag and NeuN$^+$HA-tag cells were counted.

Spine density and Sholl analyses. Spine density was analyzed for newborn neurons (32 dpi) labeled by tdTomato fluorescence. DG sections were obtained from ChR2-YPF and yellow fluorescent protein (YFP) control Ascl1CreER-Ai9 mice 32 days post tamoxifen injection. The tdTomato signal was recorded by confocal microscopy (Olympus FLUOVIEW3000; ×60 objective, 3 × zoom-in, *XY* resolution 0.4975 mm per pixel, *Z*-resolution 0.5 µm per slice). Four mice per experimental group were analyzed for dendritic spines. For each mouse, 20 dendritic fragments of 10 µm in length were quantified ($n = 80$ fragments per group). Distal dendritic fragments in the middle-to-outer molecular layer were selected. To compute spine density, the number of spines counted on each fragment was normalized by the cylindrical approximation of the surface of the specific fragment[58,59]. Experiments were conducted blind to the experimental group. Researcher 1 imaged dendritic fragments and randomized images while researcher 2 performed manual spine counting.

For 16 dpi immature neurons (tdTomato was stained with anti-RFP), Sholl analysis was performed in ImageJ by counting the number of crossings by dendrites of concentric circles originating at the soma with increasing radii of 10 µm[22]. Sholl analysis data were analyzed using two-way analysis of variance (ANOVA), with distance from the soma and ChR2/YFP groups as independent variables. Additionally, total dendritic length and number of dendrite branches of tdTomato$^+$ immature neurons (54 cells from YFP control mice and 53 from ChR2 mice) were counted.

Preparation of acute brain slices. Animals were deeply anesthetized with isoflurane and perfused intracardially with oxygenated ice-cold *N*-methyl-D-glucamine (NMDG) solution containing (in mM): 92 NMDG, 30 $NaHCO_3$, 25 glucose, 20 HEPES, 10 $MgSO_4$, 5 sodium ascorbate, 3 sodium pyruvate, 2.5 KCl, 2 thiourea, 1.25 NaH_2PO_4 and 0.5 $CaCl_2$ (pH 7.3, 310 mOsm). Slice preparation was performed in ice-cold NMDG solution. Transverse hippocampal slices (250 µm thick) were prepared using a Leica VT1200S vibratome and warmed to 34.5 °C for 8 min. Slices were subsequently maintained in HEPES holding solution containing (in mM): 92 NaCl, 30 $NaHCO_3$, 25 glucose, 20 HEPES, 5 sodium ascorbate, 3 sodium pyruvate, 2.5 KCl, 2 thiourea, 2 $MgSO_4$, 2 $CaCl_2$ and 1.25 NaH_2PO_4 (pH 7.3, 310 mOsm) at room temperature until recordings were performed.

Patch-clamp recordings. Electrophysiological recordings were carried out at 32 °C using a heater controller (TC-324C, Warner Instruments) in ACSF containing (in mM): 125 NaCl, 26 $NaHCO_3$, 20 glucose, 2.5 KCl, 2 $CaCl_2$, 1.3 $MgSO_4$ and 1.25 NaH_2PO_4 (pH 7.3, 310 mOsm). Nestin-GFP$^+$ neurons within the SGZ were visualized by differential interference contrast and fluorescence microscopy. Patch pipettes with a resistance of 5–7 MΩ were pulled from borosilicate glass capillaries (World Precision Instruments) using a micropipette puller (PC-10, Narishige). Pipettes were filled with an internal solution containing the following (in mM): 130 K-gluconate, 20 HEPES, 4 $MgCl_2$, 4 Na-ATP, 2 NaCl, 0.5 EGTA and 0.4 Na-GTP (pH 7.2, 290 mOsm). To record corelease of GABA and glutamate currents under the voltage-clamped mode, we used a cesium methanesulfonate (Cs)-based intracellular solution containing (in mM): 127.5 CH_3O_3SCs, 7.5 CsCl, 2.5 $MgCl_2$, 0.6 EGTA, 10 HEPES, 4 ATP-Na_2, 0.4 GTP-Na_3 and 10 phosphocreatine Na (pH 7.25, 290 mOsm). Because the reversal potential of Cl^- is nearly −60 mV, it is possible to detect both outward GABAergic (holding at +5 mV) and inward glutamatergic currents (holding at −60 mV). We also used a KCl-based, high-Cl^- internal solution (in mM): 140 KCl, 8 HEPES, 3 EGTA and 4 ATP-Na2, to record photo-evoked postsynaptic currents (holding at −65 mV). In some experiments, biocytin (0.2%, Sigma) was added to the internal solution to mark the recorded neuron for later morphological characterization.

Recordings were conducted in whole-cell configuration using a Multiclamp 700B amplifier (Axon Instruments). Signals were filtered at 1 kHz and sampled at 10 kHz using the Digidata 1440 A (Axon Instruments); data acquisition and pulse generation were performed using pClamp 10.7 (Axon Instruments). When needed, 100 µM D-APV, 20 µM NBQX, 100 µM AIDA and 20 µM BIC were added to block NMDA, AMPA, group 1 mGlu and $GABA_A$ receptors, respectively. Series resistance (R_s) was monitored throughout all experiments, and cells with R_s changes >20% were discarded.

Electrophysiological identification of two subtypes of nestin-GFP$^+$ cells in the SGZ. Nestin cells were identified by green fluorescent protein (GFP) in Nestin. As described previously[60], nestin-GFP-expressing cells fell into two categories based on their morphological and electrophysiological properties. Morphologically, two subpopulations of nestin-GFP$^+$ cells are distinguishable: type 1 cells have an elaborate tree of processes spanning the entire granule cell layer whereas type 2 cells have shorter, or no, horizontal processes. Compared with type 1 cells, the soma of type 2 cells tended to be smaller. Whole-cell, voltage-clamped recordings were obtained from fluorescence-labeled cells. The cell was clamped from a holding potential of −65 mV to a series of 50-ms voltage steps ranging from −13 to +25 mV at 20-mV increments. Electrophysiological examination of nestin-GFP+ cells on acutely isolated hippocampal slices showed that type 1 cells expressed passive, noninactivating currents with a linear current–voltage relationship while type 2 cells displayed outward rectification of the current–voltage curve (Extended Data Fig. 1a,b).

Contextual fear-conditioning behavior protocol. Contextual fear-conditioning experiments were carried out in a commercial fear-conditioning system (Med Associate). The context is a 29 × 25 × 22 cm^3 chamber with grid floors, opaque ceilings and white lighting. Before fear conditioning, mice were habituated to investigator handling for 5 min on three consecutive days in the holding room where the mice were housed. On day 1 mice were habituated in the behavioral context for 3 min, followed by two foot shocks (0.65 mA, 2 s) delivered at 180 and 240 s. Mice remained in the behavior chamber for 80 s after the second foot shock and were then returned to their home cages[61]. Memory retrieval was performed at 2 h, 24 h and 1 week after encoding in either the conditioned context (A) or a different context (B: white plastic floors, curved walls with visual cues and white lightning) for 5 min to recall memory. To minimize animal numbers, the same cohort of mice was used for CFC tests—that is, 13 hM3Dq-flox mice and 12 Ascl1-hM3Dq mice were used to test whether the activity of ABNs is sufficient for memory retrieval (Extended Data Fig. 7). Each mouse was injected with CNO three times for the CFC test at 1.5 h, 24 h and 7 days after training. Behavior videos were recorded with VideoFreeze software and the freezing level was automatically analyzed by the software. The chamber was cleaned with 75% alcohol or scented with 1% acetic acid to render it different to the original conditioning context.

NPR task. NPR tests were performed in a 45 × 45 × 45 cm^3 open box constructed of gray polyvinyl chloride and based on a previous study[25]. In brief, the encoding phases were identical for the NPR task and comprised a 5-min interval during which mice were allowed to explore two identical objects in the open field. After the encoding phase, mice spent 24 h in their home cage to allow memory consolidation. To test retrieval in the NPR task, one of the two objects from the encoding phase was moved to a different location. CNO was administrated by i.p. injection 30 min before memory retrieval. At each test, mice had 5 min to explore the arena. Through the open upper side of the arena, mice could perceive distal cues. Objects for exploration were glass cylinders (height 4 cm, base diameter 1.5 cm) that were stuck to the arena floor to prevent mice from moving them. Objects were positioned at least 5 cm equidistant from the walls and at least 25 cm from each other. Only those mice that showed no preference for objects in the encoding phase were included in behavior analysis. Object exploration was

considered whenever the mouse sniffed the object or touched it while looking at it (when the distance between its nose and the object was <1 cm). Climbing onto the object did not qualify as exploration. Times were converted into a discrimination ratio according to the general formula: (time at novel − time at old)/(time at old + time at novel), where novel refers to the novel position of the object. Any mice exploring both objects fewer than three times or that did not explore any object were excluded from the analysis.

Open field test. The open field test apparatus was a Plexiglas-squared arena ($45 \times 45\ cm^2$) with gray walls (40 cm high) and an open roof, which was located in a sound-attenuated and dimly illuminated room. Mice were gently placed in the center of the field, and movement was recorded for 5 min with a video-tracking system. Time spent in the center of the arena (defined as a $25 \times 25\ cm^2$ zone in the center of the apparatus) was measured[56,62]. Locomotion and time spent in the central area were analyzed by EthoVision XT (Noldus). After each trial, the apparatus was cleaned with a damp tissue containing 75% ethanol.

Forced swimming test. The apparatus for this test consisted of an acrylic cylinder (diameter 20 cm, height 30 cm) filled with water to a depth of 20 cm and maintained at 23 ± 1 °C. Each mouse was subjected to a 5-min videotaped swimming trial and subsequently analyzed by two independent observers who were blinded to the treatment. Time of immobility was reported as the mouse remained immobile during the test session. After each trial, the apparatus was filled with fresh water.

Zero maze test. The apparatus comprised a white ring (width 6 cm, outer diameter 45 cm) containing four equal quadrants of alternating walled (closed) or unwalled (open) sections. The entire ring was elevated to a height of 40 cm. Each animal was placed in the closed section at the start of the 5-min session. All test parameters were recorded and time spent in the open sections was counted. After each trial, the maze was cleaned with a damp tissue containing 75% ethanol.

Statistics and reproducibility. Data are reported and presented as mean ± s.e.m. No statistical methods were used to predetermine sample sizes, but our sample sizes are similar to those reported in previous publications[22,25,56,57]. Data distribution was assumed to be normal, but this was not formally tested. Animals or data points were not excluded and each experiment was repeated two or three times. Both behavioral analysis and cell counting were performed blinded to the conditions of the experiments. To compare cell density, spine density, discrimination ratios, freezing percentage and other behavioral tests in different groups, we used unpaired or paired *t*-tests. In SuM ablation experiments, two-way ANOVA was used followed by Tukey's post hoc test. Testing was always performed two-tailed with $\alpha = 0.05$. NS indicates no significant difference ($P > 0.05$). Statistical analyses were performed in GraphPad Prism8.

Reporting Summary. Further information on research design is available in the Nature Research Reporting Summary linked to this article.

Data availability

The authors confirm that the data supporting the findings of this study are available within the article and its supplementary materials. Source data are provided with this paper.

References

56. Li, Y. D. et al. Ventral pallidal GABAergic neurons control wakefulness associated with motivation through the ventral tegmental pathway. *Mol. Psychiatry* **26**, 2912–2928 (2021).
57. Luo, Y. J. et al. Nucleus accumbens controls wakefulness by a subpopulation of neurons expressing dopamine D1 receptors. *Nat. Commun.* **9**, 1576 (2018).
58. Roy, D. S. et al. Memory retrieval by activating engram cells in mouse models of early Alzheimer's disease. *Nature* **531**, 508–512 (2016).
59. Ryan, T. J., Roy, D. S., Pignatelli, M., Arons, A. & Tonegawa, S. Memory. Engram cells retain memory under retrograde amnesia. *Science* **348**, 1007–1013 (2015).
60. Filippov, V. et al. Subpopulation of nestin-expressing progenitor cells in the adult murine hippocampus shows electrophysiological and morphological characteristics of astrocytes. *Mol. Cell Neurosci.* **23**, 373–382 (2003).
61. Zhang, X., Kim, J. & Tonegawa, S. Amygdala reward neurons form and store fear extinction memory. *Neuron* **105**, 1077–1093 (2020).
62. Li, Y. D. et al. High cortical delta power correlates with aggravated allodynia by activating anterior cingulate cortex GABAergic neurons in neuropathic pain mice. *Pain* **161**, 288–299 (2020).

Acknowledgements

We thank all members of the Song laboratory for comments and discussions, with special thanks to B. Asrican for making the final edits of the manuscript. We also thank B. Roth for providing floxed hM3Dq and hM4Di lines for this study. This work was supported by grants awarded to J.S. from NIH (nos. R01MH111773-01, R01MH122692-01, RF1AG058160-01 and R01NS104530-01) and the Alzheimer's Association. Y.-D.L. was partially supported by a NARSAD Young Investigator Grant from the Brain & Behavior Research Foundation (no. 29600). Z.-K.C. was partially supported by grants-in-aid for scientific research from the National Natural Science Foundation of China (no. 8202010801). Z.-L.H. was supporred by the National Key Research and Development Program of China (no. 2020YFC2005300). Confocal microscopy was performed at the UNC Neuroscience Microscopy Core Facility (RRID: SCR_019060) with technical assistance from M. S. Itano. The UNC Neuroscience Microscopy Core was supported in part by funding from NIH-NINDS Neuroscience Center Support Grant no. P30 NS045892 and NIH-NICHD Intellectual and Developmental Disabilities Research Center Support Grant no. U54 HD079124.

Author contributions

J.S. supervised the project, designed the experiments and wrote the paper. Y.-D.L. designed the experiments, wrote the paper and carried out all aspects of in vivo experiments and data analysis. Y.-J.L. carried out all aspects of in vitro slice electrophysiology and helped with data analysis and preparation of the manuscript. Z.-K.C. and Z.-L.H. performed in vivo multichannel recording and related data analysis. L.Q. and L.Z. assisted with experiments and analysis. Y.C. and M.L. prepared the AAVs with genetic knockdown of Vgat or Vglut2. All authors discussed the manuscript.

Competing interests

The authors declare no competing interests.

Additional information

Extended data is available for this paper at https://doi.org/10.1038/s41593-022-01065-x.

Supplementary information The online version contains supplementary material available at https://doi.org/10.1038/s41593-022-01065-x.

Correspondence and requests for materials should be addressed to Juan Song.

Peer review information *Nature Neuroscience* thanks Masanobu Kano and the other, anonymous, reviewer(s) for their contribution to the peer review of this work.

Reprints and permissions information is available at www.nature.com/reprints.

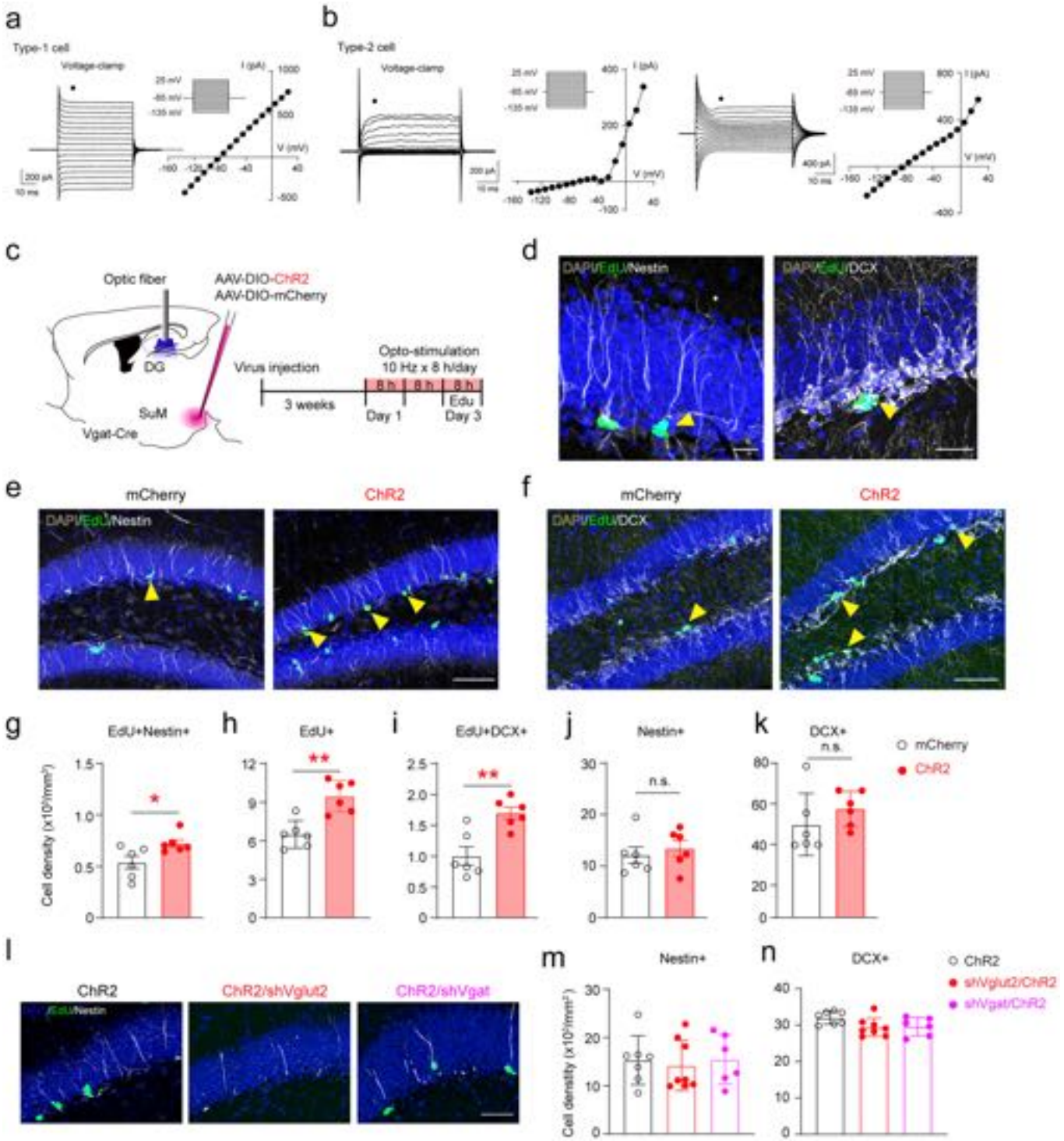

Extended Data Fig. 1 | SuM glutamate promotes proliferation of rNSCs and newborn progeny. (**a**–**b**) Nestin-GFP-expressing cells in the SGZ show distinct electrophysiological properties. Membrane currents from the nestin-GFP positive cells shown in the left column were evoked by 50-ms voltage steps ranging from −135 mV to +25 mV from a holding potential of −65 mV (the recording protocol see the inset). From these recordings, corresponding current-voltage curves were obtained at the time points indicated by the black circle above the traces (right columns). (**a**) Example for a type-1 cell expressing passive, non-inactivating currents with a linear current-voltage relationship. (**b**) Examples for two type-2 cells expressing outwardly rectifying currents, but with different reversal potentials (around −40 mV in the left, and −80mV in the right). (**c**) Diagram and stimulation paradigm for optogenetic manipulation of SuM^{Vgat}-DG projections. (**d**) Sample images of EdU/Nestin and EdU/DCX staining in the DG. Scale bar = 20 μm. (**e**–**f**) Sample images of EdU/Nestin (**e**) and EdU/DCX (**f**) staining after optogenetic activation of SuM^{Vgat}-DG projections. Scale bar = 100 μm. **g**–**k**) Density of EdU+/Nestin+ (**g**), EdU+ (**h**), EdU+/DCX+ (**i**), total Nestin+ (**j**) and total DCX+ (**l**) cells in the whole DG after optogenetic activation of SuM^{Vgat}-DG projections. n = 6 mice in each group, two-sided unpaired *t*-test, **g:** $P = 0.0099$, **h:** $P = 0.0012$, **i:** $P = 0.0029$, **j:** $P = 0.5730$, **i:** $P = 0.3101$, respectively. (**l**) Sample images of EdU/Nestin staining upon optogenetic stimulation of SuM^{Vgat}-DG projections with expressing shVgat or shVglut2. Scale bar = 50 μm. (**m**–**n**) The density of total Nestin+ (**m**) and total DCX+ (**n**) cells in the whole DG after optogenetic activation of SuM^{Vgat}-DG projections with expressing shVgat or shVglut2 in the SuM. n = 7, 8, 6 mice in ChR2, shVglut2/ChR2 and shVgat/ChR2 group, respectively. $P > 0.05$ by one-way ANOVA.

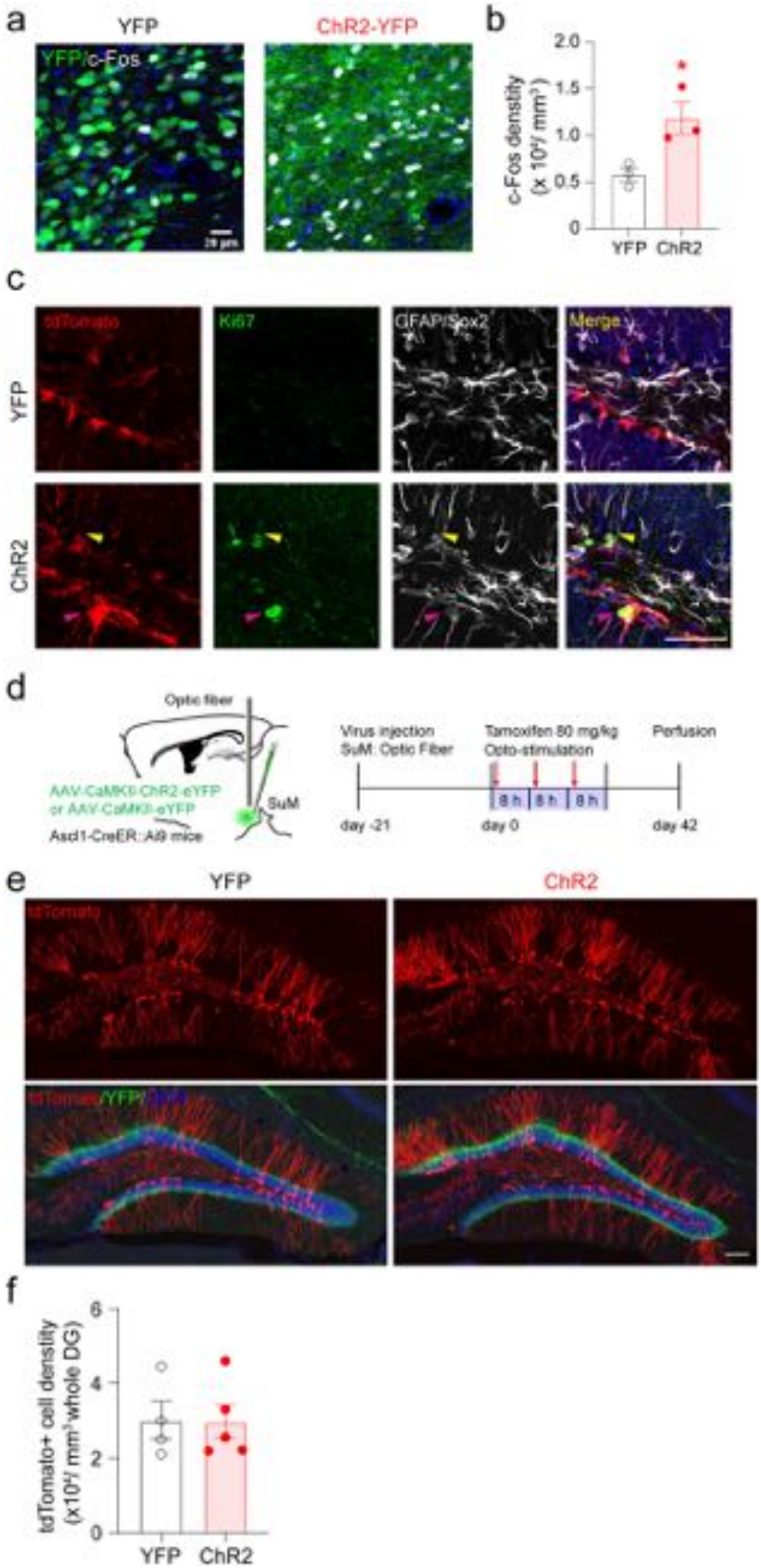

Extended Data Fig. 2 | See next page for caption.

Extended Data Fig. 2 | Short-term optogenetic activation of SuM neurons in Ascl1-Ai9 mice. (**a**–**b**) Optogenetic activation increased c-Fos expressions in the SuM. n = 3 mice for each group, $P = 0.0309$ by two-sided unpaired *t*-test. (**c**) Sample images of tdTomato+, Ki67+ and GFAP+/Sox2+ staining in the DG after optogenetic stimulation of SuM. The yellow arrow head indicated a Ki67+/tdTomato+/GFAP+ cell; the pink arrow head indicated a Ki67+/tdTomato+/Sox2+ cell. Scale bar = 100 μm. (**d**) Diagram of optogenetic stimulation of SuM neurons in Ascl1-Ai9 mice. Tamoxifen was i.p. administered at 80 mg/kg following 8 hours optogenetic stimulation of SuM neurons for 3 days. Mice were perfused on day 42 after the first tamoxifen injection. (**e**) Sample images of tdTomato+ cells in the DG at day 42 after tamoxifen injection. Scale bar = 100 μm. (**f**) The density of tdTomato+ cells in the DG. n = 4 mice for YFP group, n = 5 mice for ChR2 group, $P = 0.9558$ by two-sided unpaired *t*-test.

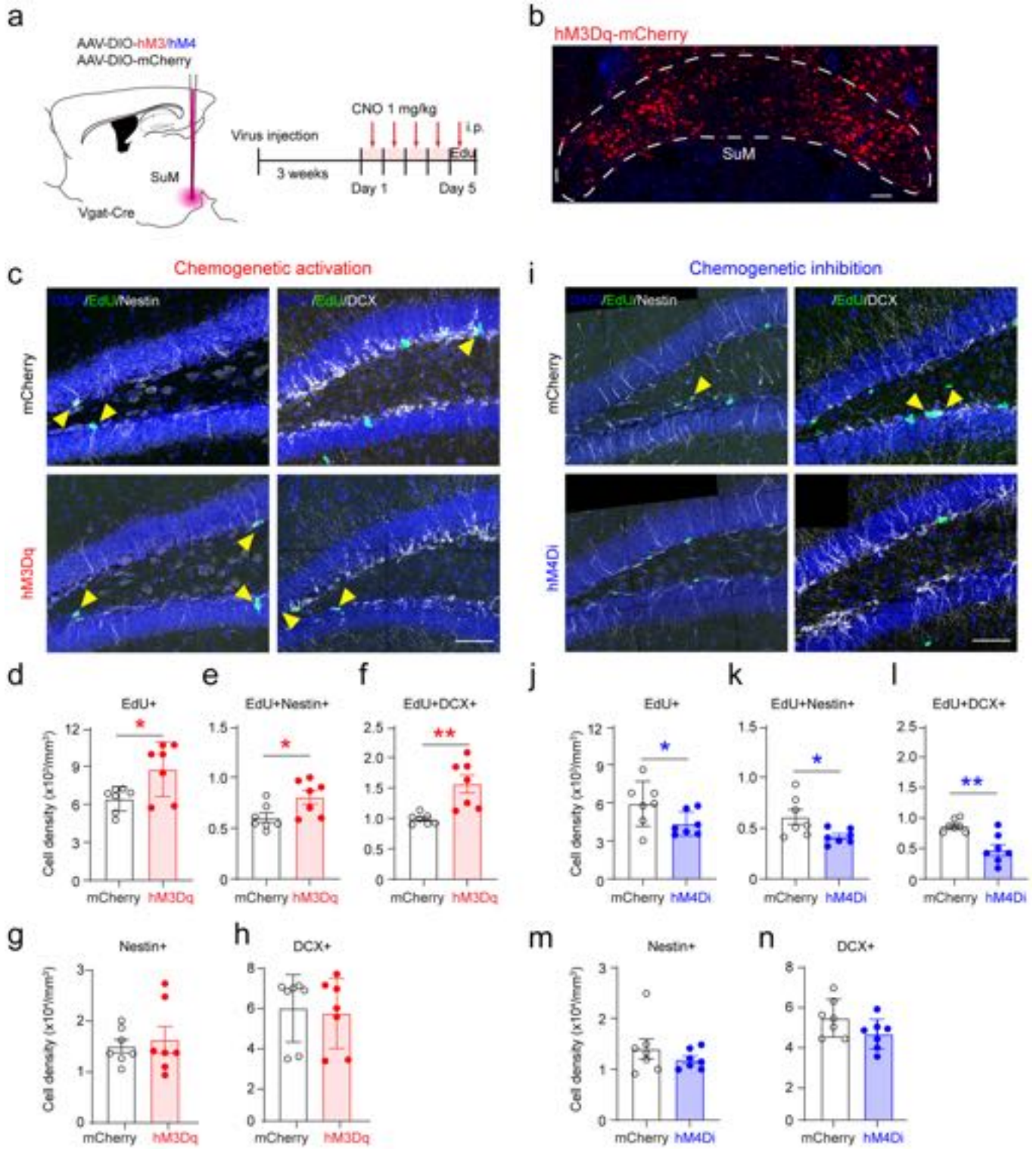

Extended Data Fig. 3 | SuM neurons are essential for the proliferation of rNSCs and newborn progeny. (**a**) Diagram of chemogenetic manipulation of SuM neurons in Vgat-Cre mice. AAV5-DIO-hM3Dq-mCherry or AAV5-DIO-hM4Di-mCherry and their control mCherry construct were bilaterally injected into SuM in the Vgat-Cre mice. After 3 weeks of virus expression, CNO 1 mg/kg was given by i.p. injection for 5 days. Mice were perfused on day 5 after 4 shoots of EdU at 40 mg/kg. (**b**) Sample image of hM3Dq-mCherry expression. Scale bar = 100 μm. (**c, i**) Sample images of EdU/Nestin (left) and EdU/DCX (right) staining after chemogenetic activation (**c**) or inhibition (**i**) of SuM^{Vgat} neurons. Scale bar = 100 μm. (**d**–**f**) Density of EdU+ (**d**), EdU+/Nestin+ (**e**), EdU+/DCX+ (**f**) in the DG after chemogenetic activation of SuM^{Vgat} neurons. n = 7 mice for each group, two-sided unpaired *t*-test, **d:** $P = 0.0225$, **e:** $P = 0.0298$, **f:** $P = 0.0012$, respectively. (**g**–**h**) Density of total Nestin+ (**g**) and total DCX+ (**h**) cells in the DG after chemogenetic activation of SuM^{Vgat} neurons. n = 7 mice for each group, two-sided unpaired *t*-test, **g:** $P = 0.6761$, **h:** $P = 0.8048$, respectively. (**j**–**l**) Density of EdU+ (**j**), EdU+/Nestin+ (**k**), EdU+/DCX+ (**l**) in the DG after chemogenetic inhibition of SuM^{Vgat} neurons. n = 7 mice for each group, two-sided unpaired *t*-test, **j:** $P = 0.0483$, **k:** $P = 0.0287$, **l:** $P = 0.0023$, respectively (**m**–**n**) Density of total Nestin+ (**m**) and total DCX+ (**n**) cells in the DG after chemogenetic inhibition of SuM^{Vgat} neurons. n = 7 mice for each group, two-sided unpaired *t*-test, **m:** $P = 0.3325$, **n:** $P = 0.1046$, respectively.

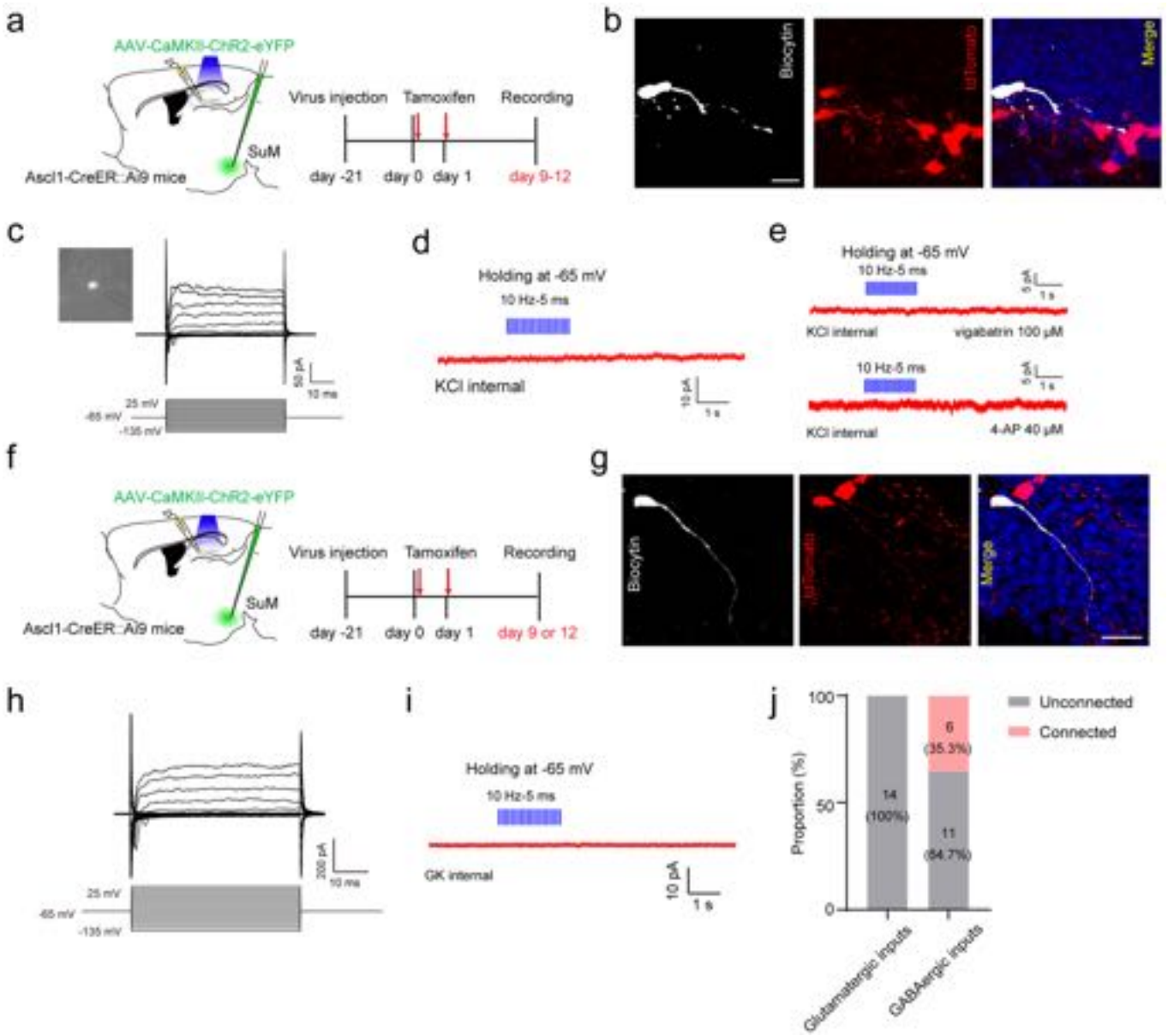

Extended Data Fig. 4 | Electrophysiological recordings of adult-born neural progenitors or neuroblasts and immature neurons. (**a**) Diagram of *in vitro* electrophysiological recording of progenitors/neuroblasts upon optogenetic stimulation of SuM-DG projections in Ascl1-Ai9 mice. (**b**) Confocal images of a biocytin-labeled tdTomato+ cell at 9 dpi after whole-cell patch clamp recording. Scale bar = 20 µm. (**c**) Electrophysiological characteristics of a neuroblast cell. Membrane currents from a non-responding cell were evoked by 50-ms voltage steps ranging from −135 mV to +25 mV at a holding potential of −65 mV. (**d**–**e**) Light stimulation failed to induce any currents in 9 dpi tdTomato+ cells, with bathing 4-AP or vigabatrin (0 of 5 cells; Vh = −65 mV; KCl-based pipette solution). (**f**) Diagram of *in vitro* electrophysiological recording of immature neurons at 9 or 12 dpi upon optogenetic stimulation of SuM-DG projections in Ascl1-Ai9 mice. (**g**) Confocal images of a biocytin-labeled tdTomato+ cell at 12 dpi after whole-cell patch clamp recording. Scale bar = 20 µm. (**h**) Electrophysiological characteristics of an immature cell at 12 dpi. Membrane currents from a non-responding cell were evoked by 50-ms voltage steps ranging from −135 mV to +25 mV at a holding potential of −65 mV. (**i**) Light stimulation failed to induce any currents in 12 dpi tdTomato+ cells (0 of 14 cells; Vh = −65 mV; GK-based pipette solution). (**j**) Proportion of connected and unconnected cells with the use of GK or KCl internal solution following blue light stimulation of SuM-DG projections. Numbers of cells are shown in parentheses.

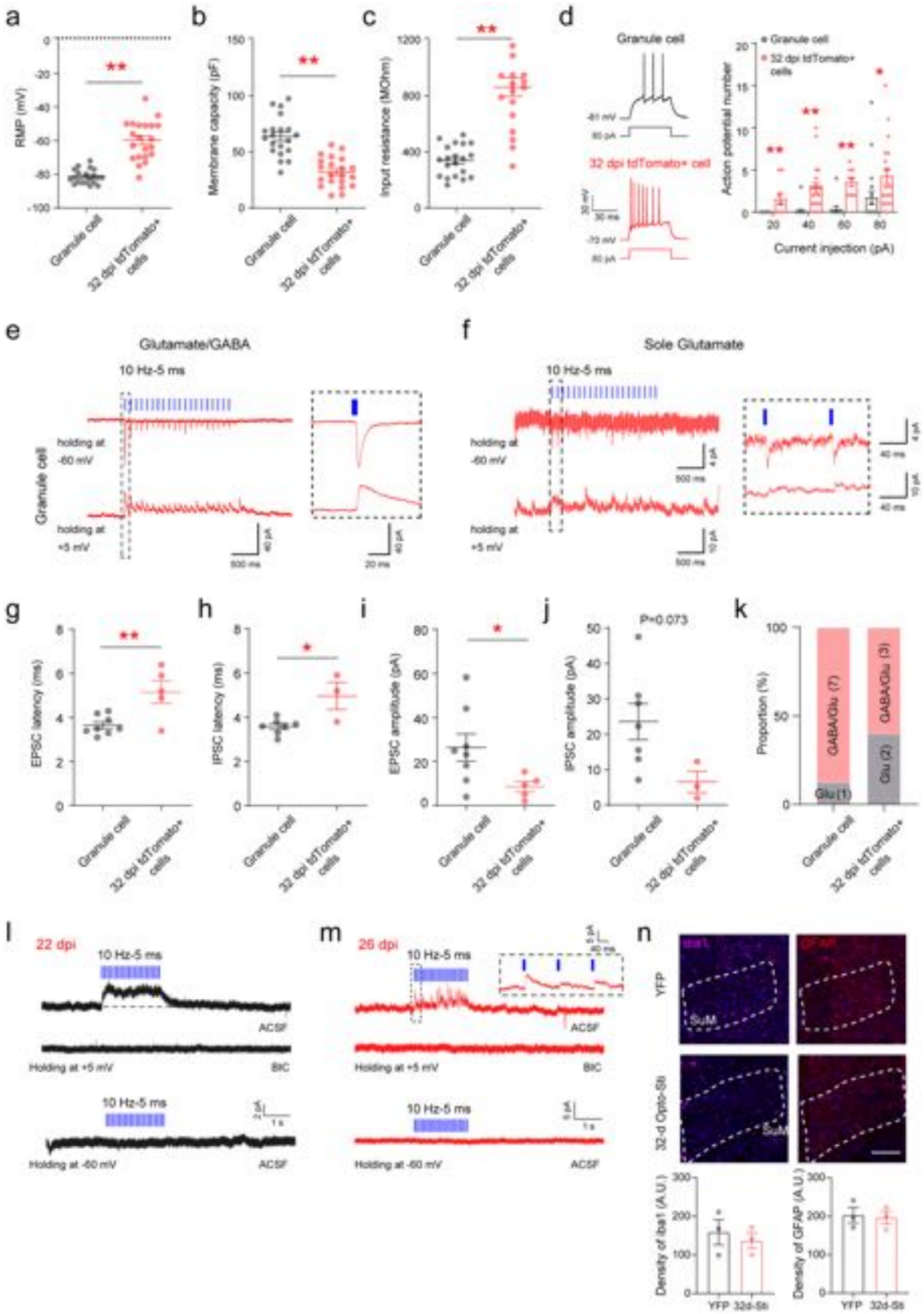

Extended Data Fig. 5 | See next page for caption.

Extended Data Fig. 5 | Adult-born neurons at 32 dpi exhibit distinct electrophysiological properties. (**a**–**c**) Comparison of intrinsic and active membrane properties in 32 dpi newborn neurons and mature GCs. Resting membrane potential (**a**), membrane capacitance (**b**), and input resistance (**c**) were measured in tdTomato+ newborn neurons and unlabeled mature GCs. n = 21 from 32 dpi newborn cells, n = 20 cells from mature GCs from 5 mice, $P < 0.0001$ by two-sided unpaired *t*-test. (**d**) The number of spikes elicited by increasing current steps in 32 dpi tdTomato+ adult-born neurons and unlabeled mature GCs. n = 20 cells for each group from 5 mice, $P < 0.0001$ by two-way ANOVA. (**e**, **f**) Sample traces showed a granule cell received both glutamate and GABA (**e**) or sole glutamate inputs (**f**) upon optogenetic activation of SuM-DG projections. (Cs-based pipette solutions). (**g**–**h**) Latency of light-evoked EPSCs (**g**) and IPSCs (**h**) in 32 dpi adult-born neurons and mature GCs. For EPSCs, n = 5 from 32 dpi newborn cells, n = 8 cells from mature GCs from 3 mice, $P = 0.0057$ by two-tailed unpaired *t*-test. For IPSCs, n = 3 from 32 dpi newborn cells, n = 7 cells for mature GCs from 3 mice, $P = 0.0117$ by two-tailed unpaired *t*-test. (**i**–**j**) Amplitude of light-evoked EPSCs (**i**) and IPSCs (**j**) in 32 dpi adult-born neurons and mature GCs. For EPSCs, n = 5 from 32 dpi newborn cells, n = 8 cells from mature GCs from 3 mice, $P = 0.05$ by two-tailed unpaired *t*-test. For IPSCs, n = 3 from 32 dpi newborn cells, n = 7 cells for mature GCs from 3 mice, $P = 0.0737$ by two-tailed unpaired *t*-test. (**k**) Proportion of glutamate and GABA inputs to GCs or tdTomato+ cells at 32 dpi following blue light stimulation of SuM-DG projections. The numbers of cells are shown in parentheses. (**l**–**m**) Newborn cells at 22 dpi (**l**) and 26 dpi (**m**) only received GABAergic inputs (Cs-based pipette solutions; Vh=+5 mV) from SuM neurons. (**n**) Sample images and quantification of iba1 and GFAP in the SuM of YFP control mice or laser stimulated (sti) mice for 32 days. n = 3 mice for each group. $P = 5939$ for (GFAP), $P = 8139$ (iba1) by two-tailed unpaired *t*-test. Values represent mean ± SEM. $^{*}P < 0.05$; $^{**}P < 0.01$ by unpaired *t*-test.

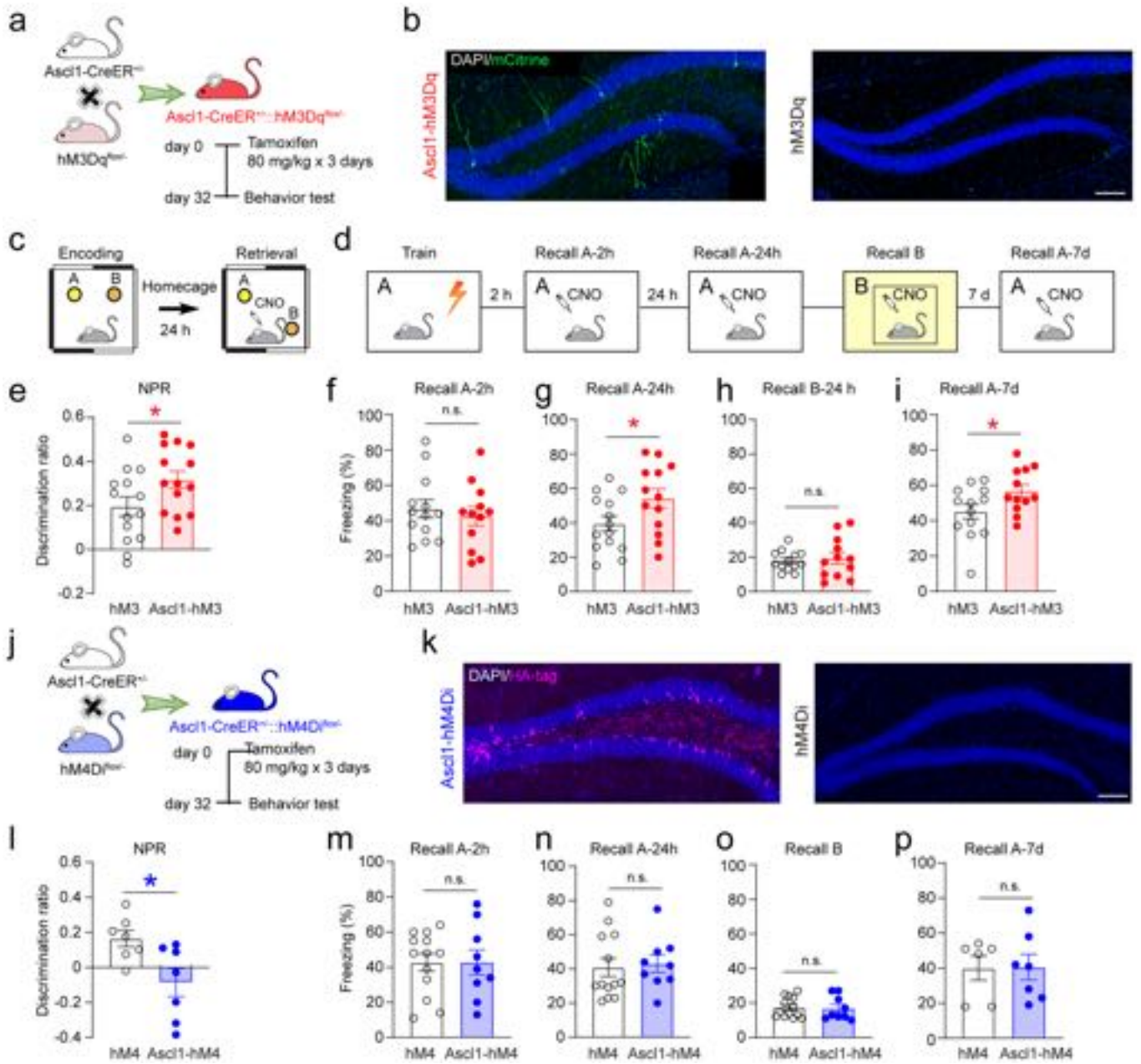

Extended Data Fig. 6 | Activity of adult-born neurons is critical for memory retrieval. (**a**) Experimental protocol for acute chemogenetic activation of adult-born neurons during behavioral tests. (**b**) Representative confocal images of mCitrine+ hM3Dq+ cells in the DG of the Ascl1-hM3Dq or hM3Dq mice. mCitrine+ cells, indicating hM3Dq+ newborn neurons, were found in Ascl1-hM3Dq mice, but not hM3Dq mice. Scale bar = 100 μm. (**c**–**d**) Diagram of NPR (C) and CFC (D) tests. (**e**) Chemogenetic activation of adult-born neurons during memory retrieval increased the discrimination ratio in the NPR test. n = 14 mice for each group, $P = 0.0484$ by two-sided unpaired *t*-test. (**f**–**i**) Freezing time in the context-A at 2 h (**f**), 24 h (**g**), in the context-B at 24 h (**h**), and in the context-A at 7 days (**i**) after chemogenetic activation of adult-born neurons. CNO 0.5 mg/kg was administrated by i.p. injection 30 mins before memory retrieval tests. n = 13 mice for hM3 group, n = 12 mice for Ascl1-hM3 group, two-sided unpaired *t*-test, **f:** $P = 0.5764$, **g:** $P = 0.0494$, **h:** $P = 0.6726$, **i:** $P = 0.0470$, respectively. (**j**) Experimental protocol for acute chemogenetic inhibition of adult-born neurons during behavioral tests. (**k**) Representative confocal images of HA+ hM4Di+ cells in the DG of Ascl1-hM4Di or hM4Di mice. Scale bar = 100 μm. (**l**) Chemogenetic inhibition of adult-born neurons decreased the discrimination ratio in the NPR test. n = 7 mice for each group, $P = 0.0202$ by two-sided unpaired *t*-test. (**m**–**p**) Chemogenetic inhibition of adult-born neurons did not change the freezing time in the CFC test. CNO 1 mg/kg was administrated by i.p. injection 30 mins before memory retrieval tests. **m**–**o:** n = 13 mice for hM4 group, n = 9 mice for Ascl1-hM4 group. **p:** n = 6 mice for hM4 group, n = 7 mice for Ascl1-hM4 group, two-sided unpaired *t*-test, **m:** $P = 0.9992$, **n:** $P = 0.7913$, **o:** $P = 0.8472$, **p:** $P = 0.9567$, respectively.

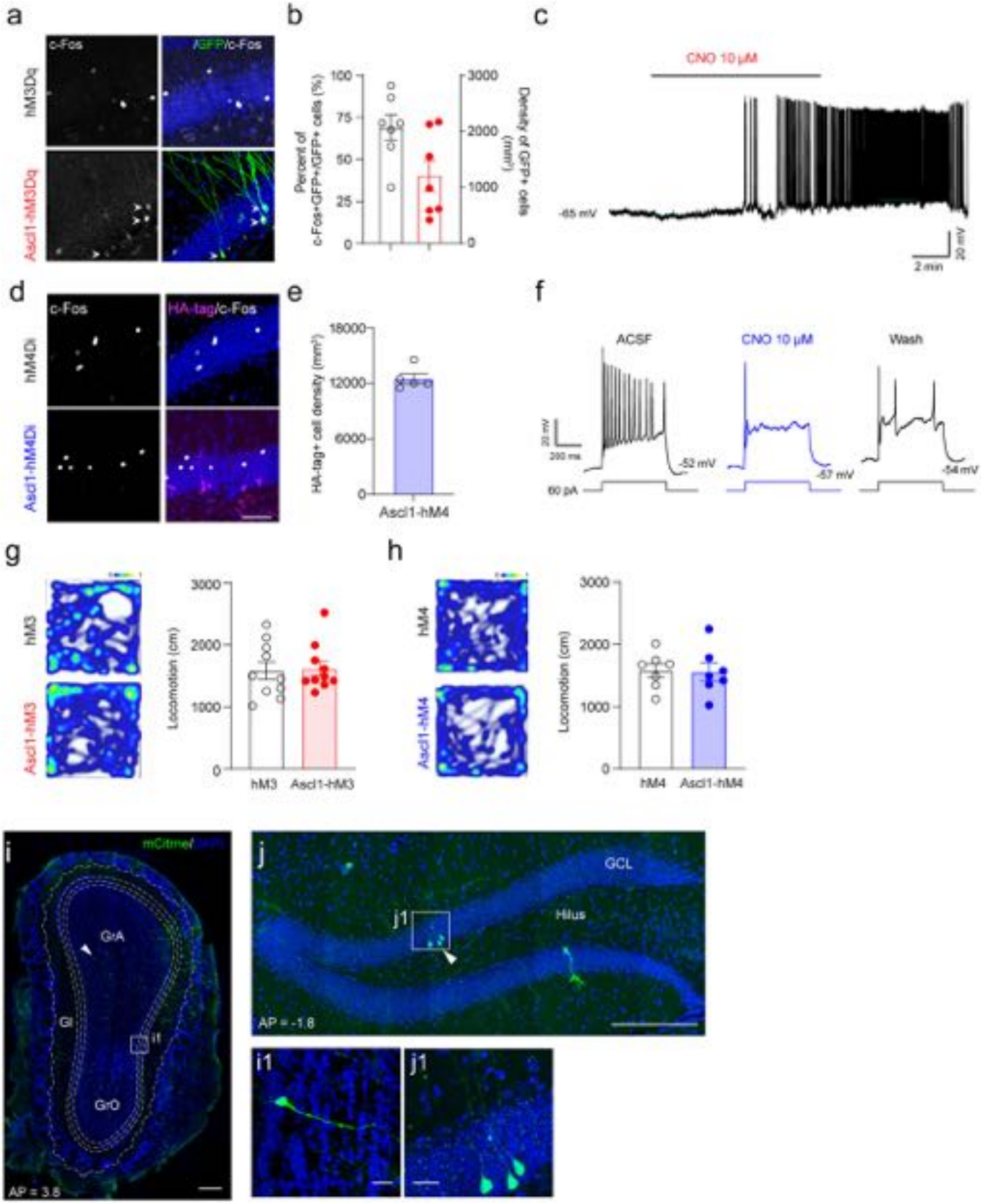

Extended Data Fig. 7 | See next page for caption.

Extended Data Fig. 7 | Chemogenetic manipulation of adult-born neurons in Ascl1-hM3Dq and Ascl1-hM4Di mice. (**a**) Representative confocal images of mCitrine and c-Fos expression in the DG of Ascl1-hM3Dq or hM3Dq mice. Scale bar = 50 μm. (**b**) Percent of c-Fos expression in mCitrine+ cells and density of mCitrine+ cells in the DG of Ascl1-hM3Dq mice after i.p. injection of CNO at 0.5 mg/kg. n = 7 mice. (**c**) Sample trace showing that bath application of CNO at 10 μM induced depolarization of membrane potential and increased firing rates in an hM3Dq+ adult-born neuron. (**d**) Representative confocal images of HA-tag and c-Fos expression in the DG of Ascl1-hM4Di or hM4Di mice after administration of CNO at 1 mg/kg. (**e**) Density of HA-tag+ cells in Ascl1-hM4Di mice. n = 5 mice. (**f**) Sample traces showing that action potentials in response to current injections in an hM4Di+ cell before, after and wash out application of 10 μM CNO. (**g**) Representative heat map of locomotion tracing for an hM3Dq control and an Ascl1-hM3Dq mouse in the NPR test (left). Quantification of total locomotion in the NPR test (right). n = 10 mice for each group, $P = 0.8410$ by two-sided unpaired *t*-test. (**h**) Representative heat map of locomotion tracing for an hM4Di control and an Ascl1-hM4Di mouse in the NPR test (left). Quantification of total locomotion in the NPR test (right). n = 7 mice for hM4 group, n = 8 mice for Ascl1-hM4 group, $P = 0.9189$ by two-sided unpaired *t*-test. (**i–j**) Ascl1 labeled ABNs were found in the OB (**i**) and DG (**j**) 32 days after tamoxifen injection. Scale bar = 100 in **i** and **j**, scale bar = 10 μm in **i1** and **j1**.

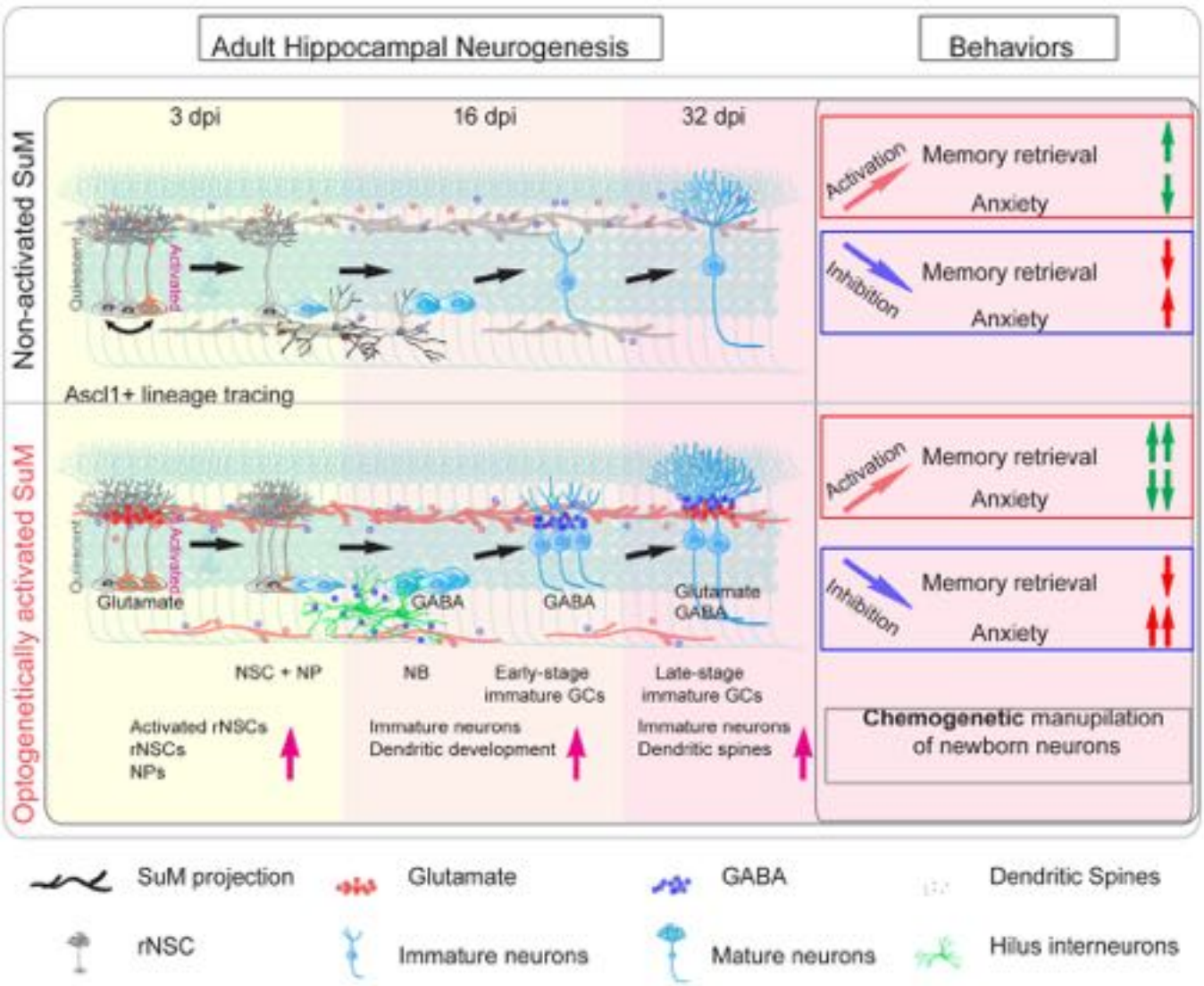

Extended Data Fig. 8 | Summary model for how circuit-modified hippocampal neurogenesis modulates hippocampal dependent behavior. By combining circuit manipulation with lineage tracing of adult-born neural precursors, we demonstrate that SuM glutamatergic inputs act on the initial rNSC stage to promote self-renewal and neurogenic proliferation of rNSCs, leading to increased production of rNSCs and neural progenitors. Then, SuM GABAergic inputs indirectly acts on the neural progenitors potentially through dentate interneurons and directly acts on early-stage immature neurons to promote differentiation of neural progenitors and dendritic development of immature neurons, respectively, leading to increased number of immature neurons with longer and more elaborate dendrites. Finally, SuM GABAergic and glutamatergic inputs collectively act on late-stage immature neurons, leading to increased number of ABNs with enhanced maturity and increased dendritic spines. Therefore, stimulating SuM neurons leads to not only increased number of ABNs, but also enhanced developmental features of ABNs. Importantly, selectively manipulating the activity of circuit-modified ABNs further modulates memory performance and anxiety-like behavior as compared to activity-manipulation of control ABNs: activation of these circuit-modified ABNs further improves memory retrieval and reduces anxiety; while inhibition of these neurons exacerbates anxiety without affecting memory performance.

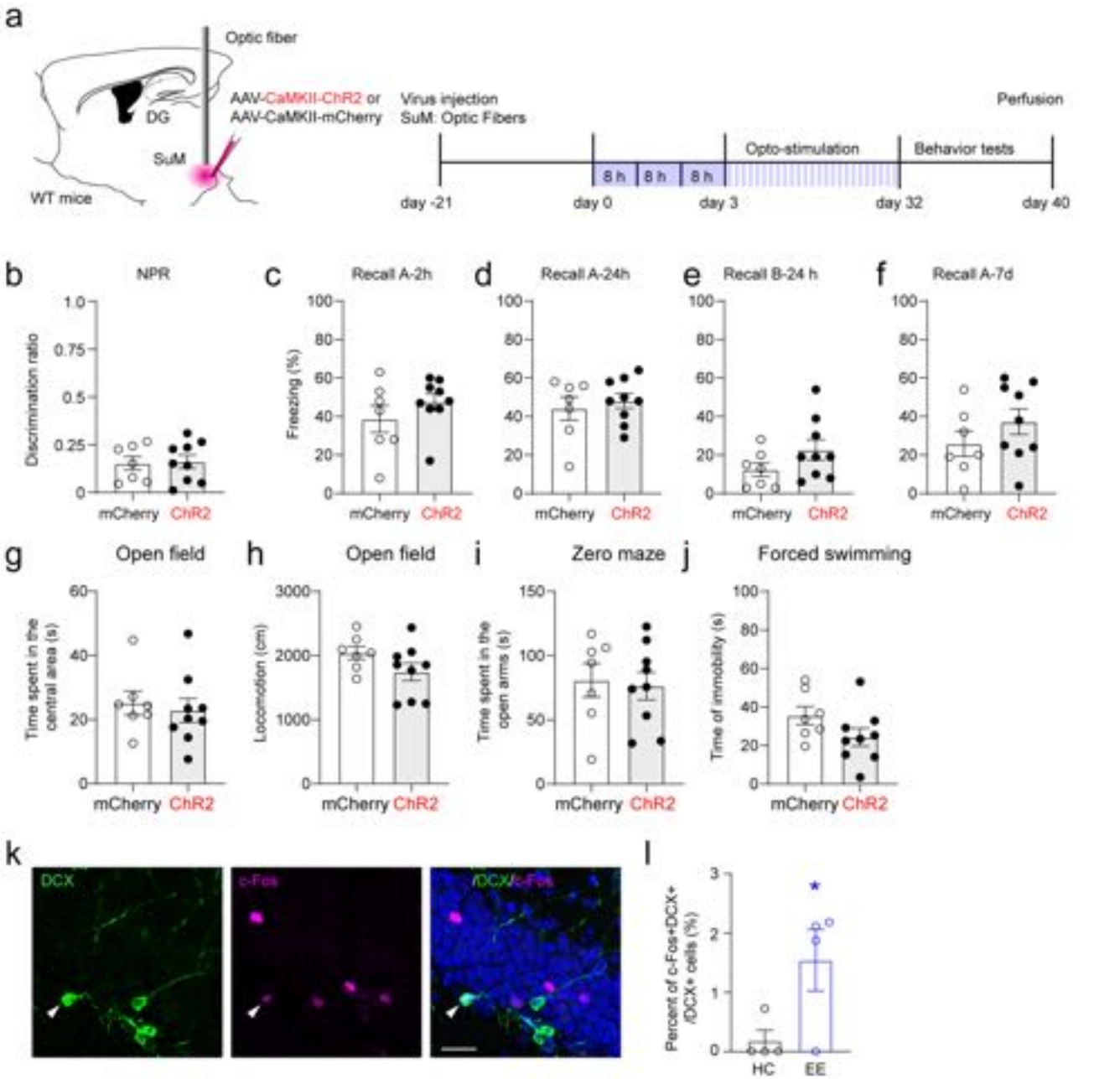

Extended Data Fig. 9 | Circuit-modified adult-born neurons do not further modulate behavior without activity manipulation. (**a**) Experimental protocol of optogenetic stimulation of SuM neurons for 32 days in wild-type mice. (**b**) Optogenetic stimulation of SuM neurons for 32 days did not change the discrimination ratio during the NPR test. n = 7 mice for mCherry group, n = 9 mice for ChR2 group, $P = 0.8550$ by two-sided unpaired *t*-test. (**c–f**) Optogenetic stimulation of SuM neurons for 32 days did not change freezing time during the CFC test. n = 7 mice for mCherry group, n = 9 mice for ChR2 group, two-sided unpaired *t*-test, **c:** $P = 0.2851$, **d:** $P = 0.5718$, **e:** $P = 0.1534$, **f:** $P = 0.2468$, respectively. (**g–j**) Optogenetic stimulation of SuM neurons for 32 days did not change behaviors in the open field, zero maze, and forced swimming tests. n = 7 mice for mCherry group, n = 9 mice for ChR2 group, two-sided unpaired *t*-test, **g:** $P = 0.6731$, **h:** $P = 0.1251$, **i:** $P = 0.9092$, **j:** $P = 0.1179$, respectively. (**k**) Sample image of DCX and c-Fos staining in HC or EE mice. The arrowhead indicates a c-Fos/DCX double positive cell. Scale bar: 20 μM. (**l**) Quantification of percent of c-Fos+DCX+/DCX+ cells. n = 4 mice in each group, $P = 0.0478$ by two-sided unpaired *t*-test. Values represent mean ± SEM. * $P < 0.05$ by unpaired *t*-test.

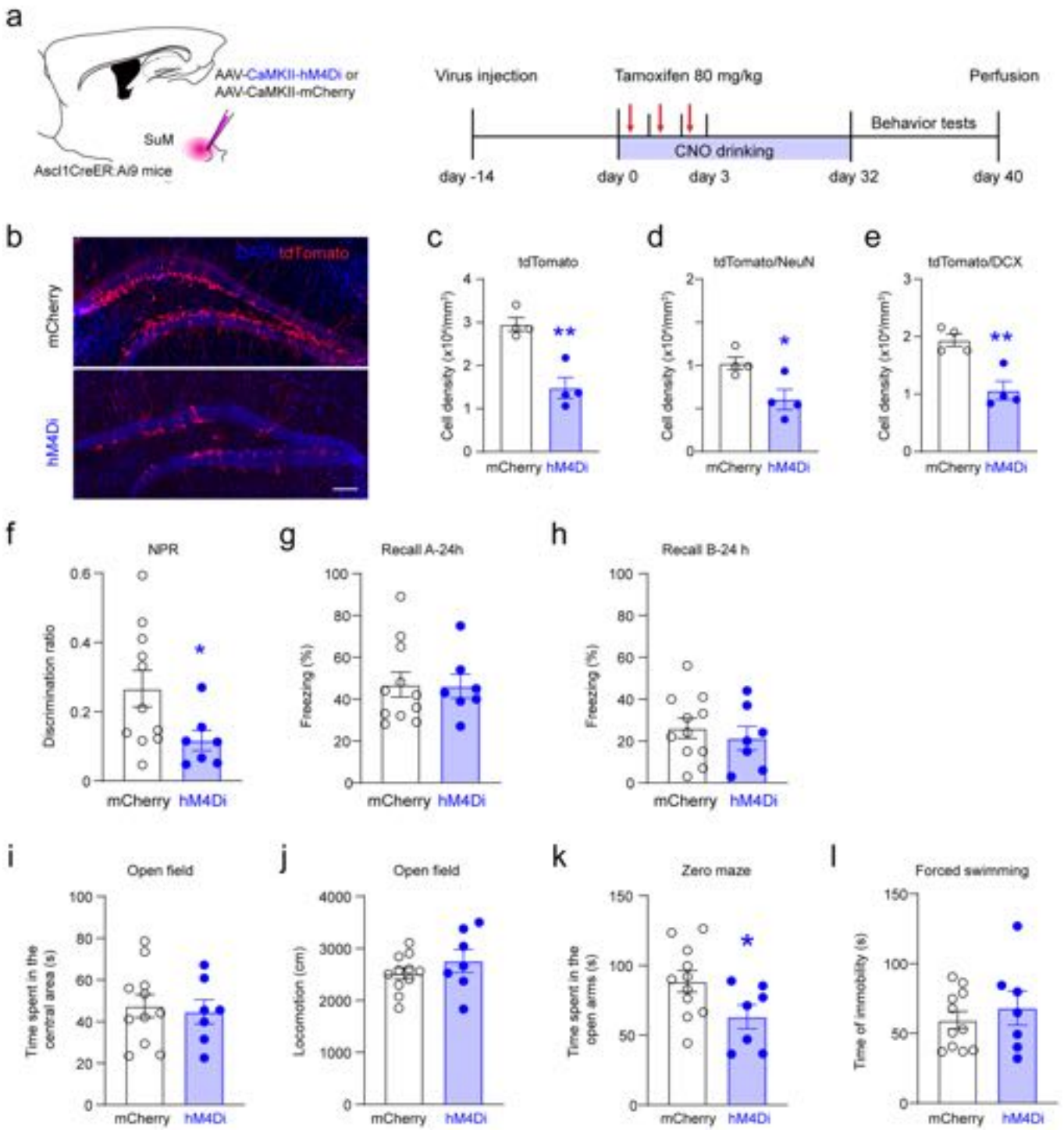

Extended Data Fig. 10 | Chronic inhibition of SuM reduced adult-born neurons and impaired hippocampal function. (**a**) Experimental protocol of chemogenetic inhibition of SuM neurons for 32 days in Ascl1CreER::Ai9 mice. Behavior tests were performed later without CNO drinking. (**b**–**c**) Chemogenetic inhibition of SuM neurons for 32 days decreased density of ABNs. n = 4 mice, $P = 0.0022$ by two-sided unpaired *t*-test. (**d**–**e**) Chemogenetic inhibition of SuM neurons for 32 days decreased density of tdTomato/NeuN+ and tdTomato/DCX+ cells. n = 4 mice, $P = 0.0234$ (**d**), $P = 0.0039$ (**e**) by two-sided unpaired *t*-test. (**f**) The discrimination ratio in the NPR test after chronic inhibition of SuM for 32 days. n = 11 mice for mCherry group, n = 7 mice for hM4Di group., $P = 0.0496$ by two-sided unpaired *t*-test. (**g**–**h**) Freezing time in the context-A and context-B at 24 hours after encoding in the CFC test after chronic inhibition of SuM for 32 days. n = 11 mice for mCherry group, n = 7 mice for hM4Di group, $P = 0.9313$ (**g**), $P = 0.5348$ (**h**) by two-sided unpaired *t*-test. (**i**–**j**) Locomotion and time spent in the central area in the open field test after chronic inhibition of SuM for 32 days. n = 11 mice for mCherry group, n = 7 mice for hM4Di group, $P = 0.3032$ (**i**), $P = 0.7419$ (**j**) by two-sided unpaired *t*-test. (**k**) Time spent in the open arms in the zero-maze test after chronic inhibition of SuM for 32 days. n = 11 mice for mCherry group, n = 7 mice for hM4Di group, $P = 0.0479$ by two-sided unpaired *t*-test. (**l**) Time of immobility in the forced swimming test after chronic inhibition of SuM for 32 days. n = 11 mice for mCherry group, n = 7 mice for hM4Di group, $P = 0.4929$ by two-sided unpaired *t*-test.

nature research

Corresponding author(s): Juan Song

Last updated by author(s): Mar 7, 2022

Reporting Summary

Nature Research wishes to improve the reproducibility of the work that we publish. This form provides structure for consistency and transparency in reporting. For further information on Nature Research policies, see our Editorial Policies and the Editorial Policy Checklist.

Statistics

For all statistical analyses, confirm that the following items are present in the figure legend, table legend, main text, or Methods section.

n/a	Confirmed	
☐	☒	The exact sample size (*n*) for each experimental group/condition, given as a discrete number and unit of measurement
☐	☒	A statement on whether measurements were taken from distinct samples or whether the same sample was measured repeatedly
☐	☒	The statistical test(s) used AND whether they are one- or two-sided *Only common tests should be described solely by name; describe more complex techniques in the Methods section.*
☐	☒	A description of all covariates tested
☐	☒	A description of any assumptions or corrections, such as tests of normality and adjustment for multiple comparisons
☐	☒	A full description of the statistical parameters including central tendency (e.g. means) or other basic estimates (e.g. regression coefficient) AND variation (e.g. standard deviation) or associated estimates of uncertainty (e.g. confidence intervals)
☐	☒	For null hypothesis testing, the test statistic (e.g. *F*, *t*, *r*) with confidence intervals, effect sizes, degrees of freedom and *P* value noted *Give P values as exact values whenever suitable.*
☒	☐	For Bayesian analysis, information on the choice of priors and Markov chain Monte Carlo settings
☒	☐	For hierarchical and complex designs, identification of the appropriate level for tests and full reporting of outcomes
☒	☐	Estimates of effect sizes (e.g. Cohen's *d*, Pearson's *r*), indicating how they were calculated

Our web collection on statistics for biologists contains articles on many of the points above.

Software and code

Policy information about availability of computer code

Data collection	FV31s-VW(Olympus FV3000), pClamp, video Freeze (Med Associates), OmniPlex Release 20.0 (Plexon Inc)
Data analysis	ImageJ (Fiji, Java 1.8.0_172), Imaris 9.8, EthoVision XT 15, GraphPad Prism 8, Offline Sorter V4.5 (Plexon Inc), NeruoExplorer V5 (Nex Technologies)

For manuscripts utilizing custom algorithms or software that are central to the research but not yet described in published literature, software must be made available to editors and reviewers. We strongly encourage code deposition in a community repository (e.g. GitHub). See the Nature Research guidelines for submitting code & software for further information.

Data

Policy information about availability of data

All manuscripts must include a data availability statement. This statement should provide the following information, where applicable:

- Accession codes, unique identifiers, or web links for publicly available datasets
- A list of figures that have associated raw data
- A description of any restrictions on data availability

The authors confirm that the data supporting the findings of this study are available within the article [and/or] its supplementary materials.

Field-specific reporting

Please select the one below that is the best fit for your research. If you are not sure, read the appropriate sections before making your selection.

☒ Life sciences ☐ Behavioural & social sciences ☐ Ecological, evolutionary & environmental sciences

For a reference copy of the document with all sections, see nature.com/documents/nr-reporting-summary-flat.pdf

Life sciences study design

All studies must disclose on these points even when the disclosure is negative.

Sample size	The sample size used in this study is based on the expected variations between animals and is comparable to many previous reports using similar techniques. Sample size of each experiments can be found in the Figure legends.
Data exclusions	Data from animals were excluded based on histological criteria that included injection sites,virus expression and optical fiber placement. Only animals with injection sites/virus expression/optical fiber placement in the region of interest were included, based on our previous reports.
Replication	All experiments were replicated 2-3 times, and all attempts at replication were successful.
Randomization	The experiments were not randomized. Animal were allocated into experimental groups by matched gender, age, weight, etc.
Blinding	Investigators were blinded to the experimental groups until all data had been collected and analyzed.

Reporting for specific materials, systems and methods

We require information from authors about some types of materials, experimental systems and methods used in many studies. Here, indicate whether each material, system or method listed is relevant to your study. If you are not sure if a list item applies to your research, read the appropriate section before selecting a response.

Materials & experimental systems

n/a	Involved in the study
☐	☒ Antibodies
☒	☐ Eukaryotic cell lines
☒	☐ Palaeontology and archaeology
☐	☒ Animals and other organisms
☒	☐ Human research participants
☒	☐ Clinical data
☒	☐ Dual use research of concern

Methods

n/a	Involved in the study
☒	☐ ChIP-seq
☒	☐ Flow cytometry
☒	☐ MRI-based neuroimaging

Antibodies

Antibodies used

Anti-Rabbit c-Fos Synaptic Systems Cat# 7-80; RRID: 226003,
Anti-Rabbit HAtag Cell Signaling Technology, #3724,
Anti-Goat GPF Rockland Cat# 600-101-215; RRID: AB_218182,
Anti-Rabbit Ki67 Thermo Fisher Scientific Cat# PA5-19462,
Anti-Goat GFAP Santa Cruz Biotechnology Cat# sc-6170,
Anti-Goat Sox2 Santa Cruz Biotechnology Cat# sc-17320,
Anti-NeuN Millipore MAB377,
Anti-Goat DCX Santa Cruz Biotechnology Cat# sc-8066,
Anti-Rabbit RFP Rockland Cat# 600-401-379,
Anti-Chicken Nestin Aves Cat# NES; RRID: AB_2314882,
Alexa Fluor 647 Goat anti-Chicken Invitrogen Cat # A32933,
Alexa Fluor 647 Donkey anti-Rabbit Invitrogen Cat # A32795,
Alexa Fluor 647 Donkey anti-Goat Invitrogen Cat # A32849,
Alexa Fluor 488 Donkey anti-Goat Invitrogen Cat # A32814,
Alexa Fluor 488 Donkey anti-Rabbit Invitrogen Cat # A32790,
Alexa Fluor 568 Donkey anti-Rabbit Invitrogen Cat # A10042,
Alexa Fluor® 647 streptavidin Thermo Fisher S21374.

Validation

All of the antibody calidation information can be found online.
Anti-Rabbit c-Fos Synaptic Systems: https://www.sysy.com/product/226008?etcc_cmp=Produkte&etcc_grp=&etcc_med=SEA&etcc_par=Google&etcc_bky=&etcc_mty=&etcc_plc=&etcc_ctv=569919801786&etcc_bde=c&etcc_var=CjwKCAiAg6yRBhBNEiwAeVyL0N0CyKrnxh7-NkQYqwvA0up9GpnivZfwlNGDDMpGDsuwt5A-

zQwJSRoCSBcQAvD_BwE&gclid=CjwKCAiAg6yRBhBNEiwAeVyL0N0CyKrnxh7-NkQYqwvA0up9GpnivZfwlNGDDMpGDsuwt5A-zQwJSRoCSBcQAvD_BwE;
Anti-Rabbit HAtag Cell Signaling Technology: https://www.cellsignal.com/products/primary-antibodies/ha-tag-c29f4-rabbit-mab/3724
Anti-Goat GPF Rockland: https://www.rockland.com/categories/primary-antibodies/gfp-antibody-600-101-215/;
Anti-Rabbit Ki67 Thermo Fisher Scientific: https://www.thermofisher.com/antibody/product/Ki-67-Antibody-clone-SP6-Recombinant-Monoclonal/MA5-14520;
Anti-Goat GFAP Santa Cruz Biotechnology: https://www.scbt.com/p/gfap-antibody-2e1;
Anti-Goat Sox2 Santa Cruz Biotechnology: https://www.scbt.com/p/sox-2-antibody-y-17;
Anti-NeuN Millipore MAB377:https://www.emdmillipore.com/US/en/product/Anti-NeuN-Antibody-clone-A60,MM_NF-MAB377;
Anti-Goat DCX Santa Cruz Biotechnology:https://www.bioz.com/result/goat%20anti%20doublecortin%20dcx%20c%2018/product/Santa%20Cruz%20Biotechnology;
Anti-Rabbit RFP Rockland:https://www.rockland.com/categories/primary-antibodies/rfp-antibody-pre-adsorbed-600-401-379/;
Anti-Chicken Nestin Aves: https://www.citeab.com/antibodies/575214-nes-nes-anti-nestin-antibody.

Animals and other organisms

Policy information about studies involving animals; ARRIVE guidelines recommended for reporting animal research

Laboratory animals	Both male and female bl6 mice were used from 6-14 weeks, transgenic mouse are listed below: VGAT-Cre (B6. Slc32a1tm2(cre)Lowl/J) mice Nestin-GFP (B6) mice Ascl1CreER (B6, Ascl1tm1.1(cre/ERT2)Jejo) mice Ai9 (B6, Gt(ROSA)26Sortm9(CAG-tdTomato)Hze) mice hM3Dq-flox (B6, Tg(CAG-CHRM3*,-mCitrine)1Ute) mice hM4Di-flox (B6, Gt(ROSA)26Sortm1(CAG-CHRM4*,-mCitrine)Ute) mice mice were used (6-14 weeks, males and females) were used for all experiments. Mice had access to food and water ad libitum and were maintained at constant temperature (22–24°C), humidity (40–60%), and 12h light/dark cycle.
Wild animals	No wild animals were used in the study.
Field-collected samples	No field collected samples were used in the study.
Ethics oversight	All procedures were conducted in accordance with the NIH Guide for the Care and Use of Laboratory Animals and with the approval of the Institutional Animal Care and Use Committee at the University of North Carolina at Chapel Hill (UNC).

Note that full information on the approval of the study protocol must also be provided in the manuscript.